Analysis of transient non-Newtonian flow of human blood

Computational Mechanics/

Analysis of transient non-Newtonian flow of blood

J.P.W. Baaijens

CIP GEGEVENS, KONINKLIJKE BIBILOTHEEK, DEN HAAG

Baaijens, J.P.W.

Analysis of transient non-Newtonian flow of human blood / J.P.W. Baaijens ; [ill. by the author]. - Eindhoven : Instituut Vervolgopleidingen, Technische Universiteit Eindhoven. - I11.
With ref.
ISBN 90-5282-178-X bound
Subject heading: human blood ; time-dependent non-Newtonian behaviour.

Analysis of transient non-Newtonian flow of blood

Author: Ir. J.P.W. Baaijens
Coaches: Prof.Dr.Ir. H.E.H. Meijer
Dr.Ir. G.W.M. Peters

Februari 1992

Post Graduate Education on Computational Mechanics
Institute for Continuing Education
Eindhoven University of Technology, Eindhoven, The Netherlands

Department of Mechanical Engineering,
Section Computational and Experimental Mechanics

WFW-report 92.023

Summary

A constitutive model has been investigated that intends to describe time-dependent non-Newtonian behaviour of human blood. It consists of an upper convected Maxwell model with parameters that are time-dependent by a separate structural kinetics equation.

Its behaviour in steady and unsteady simple shear and simple elongation flows was studied. Calculated shear stresses in simple shear flow agree well with available experimental data, in both steady and unsteady shearing.

In steady simple shear, the model produces a first normal stress difference smaller than the measurement accuracy of normal stress measurements on human blood that are reported in literature. The second normal stress difference is zero.

A five mode version of the model improves the fit of the steady viscosity curve significantly, and also fits the measured complex viscosity of human blood. However, it has two modes with singularities in the elongational viscosity. This may produce infinite elongational viscosities in for example flows with recirculation areas, which is physical incorrect. Measurements of the complex viscosity of blood in a broader frequency range are necessary to improve the multi mode fit.

In addition, the start up of steady flow of blood was calculated in a planar model of a stenosed artery at a Reynolds number of 100 and a Weissenberg number of 0.80, using the single mode model, with a Finite Element Method (a space-time, mixed Finite Element Method based on operator splitting and a Time-Discontinuous/Galerkin Least Squares method). Results are tentative, but they show that the numerical method used can succesfully be applied for this type of problem. The computer program that is now available has a large potential for future studies.

Symbols

$\boldsymbol{\mathcal{T}}$	Cauchy stress tensor	[Pa]
$\boldsymbol{\mathcal{T}}'$	extra stress tensor	[Pa]
p	pressure	[Pa]
P	structure parameter in Rosenblatt model	[-]
P^0	steady state value for P	[-]
$\boldsymbol{\mathcal{D}}$	rate of deformation tensor	[s^{-1}]
II_D	second invariant of D ($(2D:D)^{\frac{1}{2}}$)	[s^{-1}]
α	parameter Rosenblatt model	[-]
k	parameter Rosenblatt model	[s^{-1}]
C	power-law constant	[Pa s^n]
n	power law index	[-]
$\tau_{xy}, \tau_{xx}, \tau_{yy}$	components of extra stress tensor	[Pa]
τ_y	yield stress	[Pa]
η_c	Casson viscosity	[Pa s]
η^0	zero shear viscosity	[Pa s]
η^∞	infinite shear viscosity	[Pa s]
η_{0i}	zero shear viscosity in multi mode Rosenblatt model	[Pa s]
$\bar{\eta}$	elongational viscosity	[Pa s]
G	modulus	[Pa]
k_{0i}	parameter k in multi mode Rosenblatt model	[s^{-1}]
α_i	parameter α in multi mode Rosenblatt model	[-]
λi	time constant in multi mode Maxwell model	[s]
P_i	structure parameter in multi mode Rosenblatt model	[-]
N	number of modes	[-]
$\dot{\gamma}$	shear rate	[s^{-1}]
$\dot{\varepsilon}$	elongational rate	[s^{-1}]
Re	Reynolds number	[-]
We	Weissenberg number	[-]
ρ	density	[kg/m^2]

D	diameter entrance of flow geometry	[m]
$\bar{u}$	mean fluid velocity	[m/s]
u	velocity in x-direction	[m/s]
v	velocity in y-direction	[m/s]
Δt	time step	[s]
$\vec{u}(\vec{x},t)$	velocity field	[m/s]
$\vec{u}_0$	velocity on boundary	[m/s]
t	time	[s]
$\vec{x}$	position	[m]
$\vec{p}$	position of particle at time t_n that is on position $\vec{x}$ at time t_{n+1};	[m]
$\vec{\nabla}$	Nabla operator	
∇	upper convected time derivative	
$\frac{D}{Dt}$	material time derivative	
$\frac{\partial}{\partial t}$	local time derivative	
L^T	velocity gradient tensor	[s^{-1}]
S_n	space-time slab at time t_n	
Ω_n	space slab at time t_n	
I_n	time slab between t_n^+ and t_{n+1}^-	
Γ	boundary of flow geometry	
T	length of time domain	[s]
P_k	k-th order integration polynomial on a triangle	
Q_k	k-th order integration polynomial on a quadrilateral	
τ	structural part of the extra stress tensor	[Pa]
B_p	value of B (tensor,vector,scalar) of a particle that is on position $\vec{p}$	[..]
H^k	Hilbert function space of order k	
L_2	space of Lebesque square integrable functions	

Contents

1 Introduction

This report concerns the modeling of the time-dependent non-Newtonian behaviour of blood. A non-Newtonian constitutive model was investigated in several simple shear and simple elongation flows and in a planar flow with a model stenosis.

Our interest in applying this type of constitutive models for blood is raised by the study of the blood flow through the human carotid artery bifurcation. This bifurcation is the central problem in the project "Atherosclerosis", a cooperation between the Eindhoven University of Technology and the University of Limburg. Atherosclerosis is a disease that narrows blood vessels by formation of atherosclerotic plaques at the wall, particularly in arteries with bends and bifurcations. These plaques ultimately occlude the vessel, or fragments peeled of the wall can block a downstream artery. In both cases, clinical consequences are obvious. A mathematical model of the flow of blood contributes to the development of a method to diagnose the atherosclerosis in an early stage of the disease.

Calculation of the flow in the carotid artery bifurcation involves a number of problems that have to be solved: unsteadiness of the flow, three-dimensionality of the flow, elasticity of the artery wall, and non-Newtonian behaviour of the blood.

Simple shear flows are used to characterize fluid behaviour. In simple shear flows at shear rates below 100 s^{-1} it is experimentally observed that blood behaves as a non-Newtonian fluid (e.g., Thurston [1979], McMillan et al [1987]).

In steady simple shear flows a decrease of the viscosity with increasing shear rate reflects the time-independent behaviour of blood (McMillan et al [1987]). This shear thinning effect can be described with time-independent constitutive models, so called generalized Newtonian models. These models relate present stresses with present shear rates only.

In unsteady simple shear flows, blood shows not only shear thinning behaviour, but also time-dependent effects (e.g., McMillan et al [1987]). To describe these effects more complex constitutive models that take into account the history of deformation have to be used.

Many studies, both numerically and experimentally, report about the flow in the human carotid artery bifurcation (Ku and Giddens [1987], Van de Vosse [1987], Rindt [1989], Reuderink [1991]), making different simplifying assumptions. In general, it is assumed that blood behaves as a Newtonian fluid.

The Newtonian assumption is justified by two arguments. First, in steady shear flows the shear viscosity gets a constant value at shear rates above about 100 s^{-1}, while in large arteries in the human body maximal shear rates above 500 s^{-1} are typical. Thus the Newtonian assumption seems to be realistic in those cases.

However, many (Newtonian) studies (e.g., Ku and Giddens [1987], Rindt [1989]) have shown that in bends and bifurcations flow areas occur with flow recirculation and low shear rates. Thus the non-Newtonian, shear thinning behaviour of blood might be of importance in these situations too. To investigate this effect, Baaijens et al [1992] used two time-independent, generalized Newtonian constitutive models for blood to calculate numerically the flow through a two dimensional model of the human carotid artery bifurcation. It was found that in these cases the general flow structure was not affected by the generalized Newtonian models used. Locally some differences with the Newtonian results were found. The results of others (e.g, Perktold [1989], Perktold et al [1989]) confirm these results. Again this confirms the Newtonian assumption as reasonable.

However, strong objections exist against the use of generalized Newtonian models in flows that have not only shearing deformation (see Chapt. 2). Also, when generalized Newtonian models are used in flows where acceleration and slowing down of fluid takes place, effects that are related with time-dependent behaviour of blood (viscoelasticity, thixotropy) are ignored. In particular in flow recirculation areas these effect might control the flow phenomena dominantly. Therefore care should be taken when making conclusions on the ground of these calculations alone.

The relevance of the time-dependent behaviour of blood has not yet been investigated well. The most important report on this is the experimental study of Mann and Tarbell [1989] who measured the wall shear stresses in a ninety-degree curved tube during oscillatory flow. They used three non-Newtonian fluids (bovine blood, a Separan solution and a Xanthan gum solution) and one Newtonian fluid (an aqueous Glycerine) as rheological analog fluids for blood. The non-Newtonian fluids all had the same shear thinning viscosity. However, significant differences were found between the wall shear stresses measured in the four cases. Also, measurements with bovine blood showed significant differences with those on the Newtonian solution. This implies that one should be careful with interpreting measurements of fluids that have the same steady shear viscosity curve.

The second reason for using a Newtonian model is the fact that no adequate constitutive models and/or mathematical tools were available to calculate the non-Newtonian flow of blood. Much more complex constitutive models have to be used in order to describe time-dependent non-Newtonian effects, but because of numerical difficulties no realistic flow calculations could be made in the past. Fortunately, recently important progress has been made in this research field that enables more realistic viscoelastic flow calculations (e.g., Hulsen [1989,1991], Baaijens [1992]). Further, measurements in two or three dimensional viscoelastic flows of the stress or the velocity field are very difficult, and in case of blood without an

appropriate rheological analog fluid even impossible.

In the recent past, several authors have proposed constitutive models that intend to describe the time-dependent behaviour of blood. One of those models is the Rosenblatt model. We chose this model for several reasons that will be discussed in Chapt. 3. As a prepatory study, we studied its behaviour in simple shear (Chapt. 4) and elongation flows (Chapt. 5). The calculated shear stresses in simple shear flow, during a loading program that consisted of two constant shearing perods of time each followed by a non-shearing time period, agree well with experimental data in case of shear rates of 8, 23 and 30 s^{-1}.

Besides shear stresses, also normal stress differences are of importance when studying viscoelastic behaviour. Only a few measurements of normal stress differences are reported in the literature. Copley and King [1975] reported such measurements in steady shear for shear rates from 0.001 to 5 s^{-1}, and could not measure any normal stress difference. Their measurement accuracy was maximal 90 mPa. Our model calculations yield a first normal stress difference that is smaller than this measurement accuracy and a second normal stress difference that is zero. Hence, our calculations do not contradict with experimental data within the measurement error.

A five mode version of the model improved the fit of the steady viscosity curve significantly. It also fitted the measured complex viscosity of human blood well. This five mode fit has a mode with a singularity in the elongational viscosity, which gives rise to unrealistic, infinite stresses in elongational deformation. This might occur in flow recirculation areas. Measurements of the complex viscosity in a broader range of frequencies may result in a better fit of the multi mode model.

Also the flow of blood in a planar model of a stenosed artery using the Rosenblatt model was calculates. These calculations have a tentative character. The results show that the numerical method used can succesfully be applied for this type of problem. The computer program now available has a large potential for future studies.

More detailed comparative studies, both numerically and experimentally, are necessary to reveal the relevance of the non-Newtonian behaviour of blood on the three dimensional time-dependent flow phenomena in the human carotid artery bifurcation.

2 Review of literature

2.1 Introduction

Blood exhibits non-Newtonian behaviour. First of all its steady viscosity decreases with shear rate ('shear thinning'). Further, numerous researches have found that blood also exhibits time-dependent behaviour, such as viscoelasticity and thixotropy. This complicated material behaviour is caused by the microstructure of blood. The review of literature first concerns the rheology of blood (Sections 2.1, 2.2). These section are meant as an introduction, for more detailed information it is referred to for example Caro et al [1978]. Second, the physiological flow situation is described (Section 2.3), and then literature concerning constitutive models for blood is discussed shortly (Section 2.4). For a more detailed review of literature it is refered to Baaijens [1991].

2.2 Rheology of blood

Blood is a suspension of blood cells and liquid particles (the chyomicrons) in the plasma. It has a specific mass of 1.050 10^3 kg/m^3. If all particles are removed from the blood and it is anticoagulated, the plasma rests. It appears from experiments (Caro et al [1978]) that plasma is a Newtonian fluid; at 37°C it has a viscosity $\eta_{plasma} = 1.2\ 10^{-3}$ Ns/m^2. The chyomicrons are 0.2 - 0.5 μm long and have such a small concentration that they do not influence the macroscopic rheological properties of blood.

Further, the blood cells can be subdivided in red and white blood cells and blood platelets. The concentration of white blood cells (leukocytes) and platelets is so low relative to the red blood cells (erythrocytes), see Table 2.1, that they are considered to be not important for the rheological behaviour of blood.

Table 2.1 Cells in blood (Caro et al [1978]).

Cells in blood

Cell	Number per mm^3	Unstressed shape and dimensions (μm)	Volume concentration (%) in blood
Erythrocyte	4–6 × 10^6	Biconcave disc 8 × 1–3	45
Leucocytes			
Total	4–11 × 10^3		
Granulocytes			
Neutrophils	1·5–7·5 × 10^3	Roughly spherical 7–22	1
Eosinophil	0–4 × 10^2		
Basophil	0–2 × 10^2		
Lymphocytes	1–4·5 × 10^3		
Monocytes	0–8 × 10^2		
Platelets	250–500 × 10^3	Rounded or oval 2–4	

The red blood cells (RBC) determine the rheology of blood. The volume concentration, also called hematocrit (HTC), is 45 %. Red blood cells contain hemoglobine, a fluid that is responsible for the oxygen transport. When the cell is not deformed, it has a concave shape (Fig. 2.1), and a specific mass of 1.08 10^3 kg/m^3 (slightly larger then for the whole blood). The cell consists of a thin membrane containing a fluid. The cell has no nucleus. The viscosity of the interior fluid is about 6 10^{-3} Ns/m^2, about 5 times the plasma viscosity.

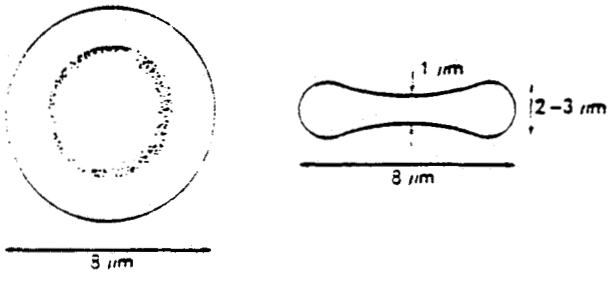

Composition of the red cell

	Percentage of mass
Water	65
Membrane components (protein, phospholipid, cholesterol)	3
Haemoglobin	32
Inorganic:	
Potassium	0·420 g per 100 ml
Sodium	0·025 g per 100 ml
Magnesium	0·006 g per 100 ml
Calcium	small amount

Figure 2.1 *The red blood cell (from Caro et al [1978]).*

The RBC has two important characteristics that influence the flow of blood. First, the cell is strongly deformable (it has a Young's modulus of order 10^5 Nm^{-2} (Bernadin [1986])), with high shear stresses it is stretched. The deformation of the red cells becomes significant for shear rates greater then 1 s^{-1}, it reaches a maximal value for $\dot{\gamma} \approx 100$ s^{-1} (Bernadin [1986]).

Secondly, at low shear rates ($\dot{\gamma} < 10$ s^{-1}, see for example Fig. 1.2) the red blood cells aggregate. This is called rouleaux formation. At very low shear rates ($\dot{\gamma} << 1$ s^{-1}, Bernadin [1986]) rouleaux can form a three dimensional network. With increasing shear rate the network is broken down, and the rouleaux are dispersed into individual cells. In this regime a structural kinetic process of competing structure break down and build up exists. For $\dot{\gamma} > 10$ s^{-1} no rouleaux exist in steady shear. Fig. 2.2 illustrates both effects. Depending on the shear stress, aggregates of undeformed cells are formed or dispersed cells are deformed.

In steady simple shear flow, blood shows shear thinning behaviour (Fig. 1.3). This can be explained as follows. At very low shear rates ($\dot{\gamma} << 1$ s^{-1}) aggregation of rouleaux to a three dimensional network causes relatively high shear stresses. With increasing shear rates, first the network is deformed and broken down; at shear rates $0.1 < \dot{\gamma} < 1$ s^{-1} the bending and orientation of the rouleaux result in a further decrease of the viscosity. At higher shear rates ($\dot{\gamma} > 1$ s^{-1}) the rouleaux are broken down, while for $\dot{\gamma} > 10$ s^{-1} no rouleaux exist and with increasing shear rate the viscosity decreases as a result of the orientation and deformation of

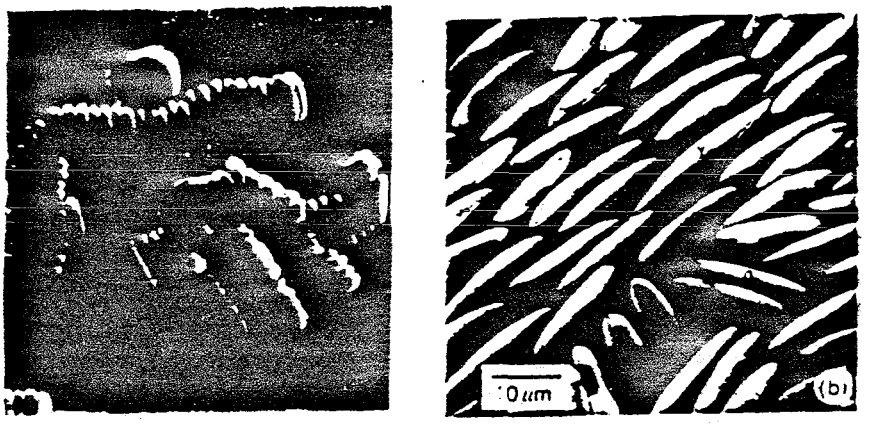

Figure 2.2 *Two states in which the RBC can exist depending on shear stress: (a) undeformed, aggregated (τ = 0 N/m^2), (b) deformed, unaggregated (τ = 300 N/m^2) (from Caro et al [1978]).*

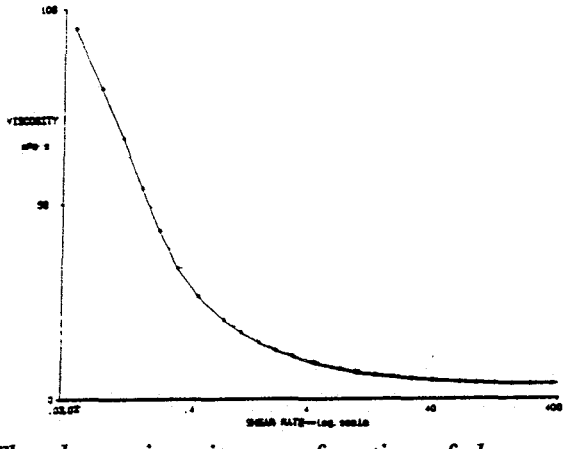

Figure 2.3 *The shear viscosity as a function of shear rate for whole human blood (HTC = 45 %) (from McMillan et al [1987]).*

the individual red blood cells. For high shear rates ($\dot{\gamma}$ > 100 s^{-1}) the viscosity becomes Newtonian. The separate influences of the deformation and aggregation on the shear viscosity of blood are illustrated in Fig. 2.4. Aggregation increases the viscosity at low shear rates, deformation decreases the viscosity at high shear rates.

The shear rate dependence of the viscosity of blood is often described by a power-law or Casson relation:

power-law: $$\eta = C\,\dot{\gamma}^{n-1} \qquad (2.1)$$

Casson: $$\eta = (\tau_y + 2\tau_y^{\frac{1}{2}}(\eta_c\dot{\gamma})^{\frac{1}{2}} + (\eta_c\dot{\gamma}))/\dot{\gamma} \qquad (2.2)$$

with η the viscosity, C the power-law constant, n the power-law index, $\dot{\gamma}$ the shear rate, τ_y the yield stress, η_c the Casson viscosity. The Casson model contains a yield stress, this is discussed in the next section. Typical parameter values for human blood are (Baaijens [1991]): C = 0.028, n = 0.63, $\tau_y = 4.8\ 10^{-3}\text{Nm}^{-2}$, $\eta_c = 2.8\ 10^{-3}\ \text{Nsm}^{-2}$.

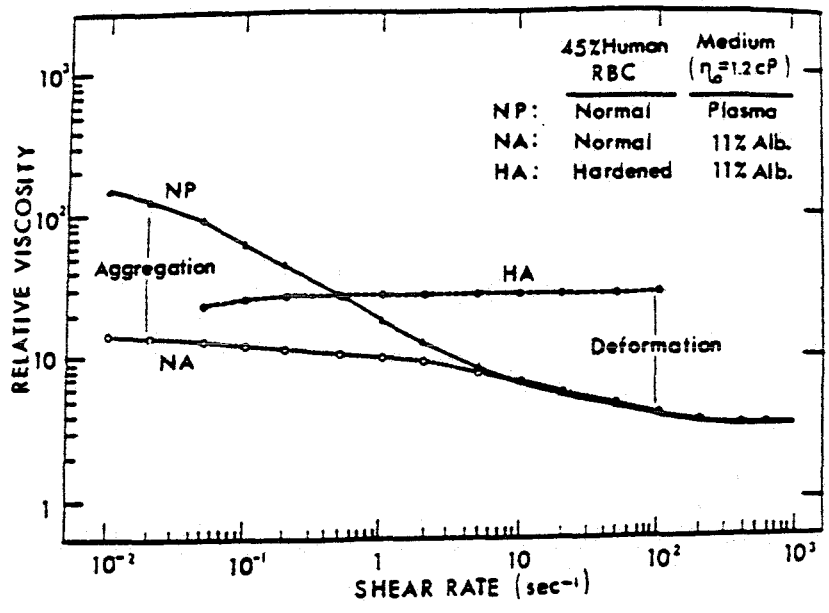

Figure 2.4 *The relative shear viscosity (η/η_0; η_0 = viscosity of the plasma = 1.2 mPas) of whole human blood (HTC = 45 %) as a function of shear rate; the contribution of deformability and aggregation is indicated. (NP = normal red cells in plasma, NA = normal red cells in isotonic saline containing 11 % albumin to prevent aggregation of the red cells; HA = hardened discoid red cells in the same saline) (from Chien [1970]).*

Yield stress

According to Caro et al [1978] blood has a yield stress of 1.5 - 5 mN/m^2. However, as discussed for example by Walburn and Schneck [1976], the yield stress was measured only under static loading conditions. It is doubtful whether the yield stress is at all manifest in a (physiological) dynamic situation.

Linear viscoelasticity

Standard measurements of linear viscoelastic behaviour are measurements of the

dynamic complex viscosity and its elastic and viscous components (Fig. 2.5). The complex viscosity is defined in a small amplitude oscillatory flow by

$$\eta^* = \tau^*/\dot{\gamma}^* = \tau_0/\dot{\gamma}_0\, e^{i\varphi} = \eta' - \eta''i \qquad (2.3)$$

The non zero elastic component η'' in Fig. 2.5 proves that blood shows viscoelastic behaviour. The relation between the complex viscosity of blood and its microstructure is elucidated by the study of Huang et al [1975]. They found that at low oscillation frequency in blood (40% HTC)

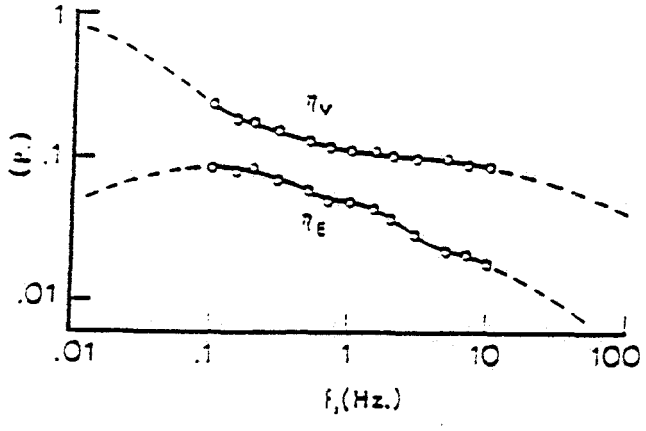

Figure 2.5 *The elastic and viscous components of the complex viscosity of whole human blood (HTC = 43 %) as a function of frequency (from Thurston [1979]).*

large rouleaux that deform elastically exist for $\dot{\gamma}_0 < 1\ s^{-1}$. This leads to a substantial elastic component of the complex viscosity. They also found that with increasing frequency above 0.1 Hz the rouleaux size decreases as well as the value of η'', probably because of the cyclic deformation. At frequencies of 1 Hz or larger hardly no rouleaux exist in the suspension. Then only the deformation and orientation of the individual red blood cells contribute to the elastic component η''. This is confirmed by Fig. 2.6 in which the complex viscosity in a RBC suspension in plasma is compared with a RBC in Albumin-Ringer. In this latter solution no aggregation can take place; it has a constant η'' that is about 5 times smaller compared with

the suspension in plasma. The difference becomes smaller when the frequency increases, a result of the disaggregation process.

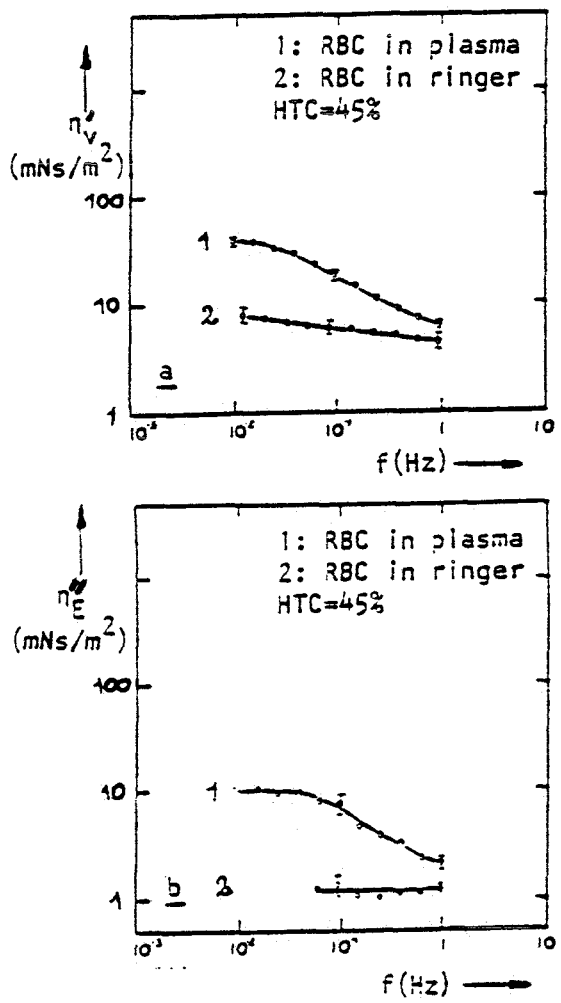

Figure 2.6 *The components of the complex viscosity as a function of frequency in plasma and in a Ringer solution (in which the red cells cannot aggregate); a) η', b) η" (from Chien [1979]).*

Thixotropy

A third aspect of non-Newtonian behaviour of blood is thixotropy. Thixotropy is the time-dependent behaviour caused by the kinetic structure processes of aggregation and disaggregation. It is experimentally observed after, for example, a repetition of shear rate steps.

When the blood is sheared from rest to a steady shear rate value, a shear stress overshoot peak is observed (Fig. 2.7). If the same shear rate step is repeated after a short period without shearing, a shear stress peak smaller than the first peak is observed. The longer the period between the two shear rate steps, the lesser the difference between the two

overshoot peaks (McMillan et al [1987]). This can be explained by the structural break down that has taken place during the first step. During the period between the two rate steps the structure is build up again. McMillan et al [1987] reported several such experiments with rate steps from 0 to 8,13,23, and 30 s^{-1}.

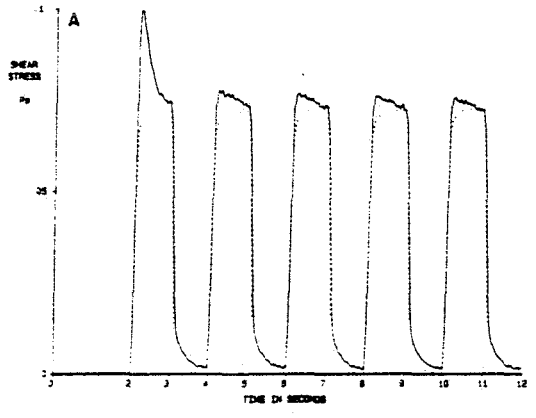

Figure 2.7 *Shear stress measurement during a simple shear experiment with 5 periods of 1 s with constant shearing at $\dot{\gamma}$ = 8 s^{-1}, divided by non shearing periods of 1 s (McMillan et al [1987])*

Normal stress differences

Reports of measurements of normal stress differences of blood are difficult to find. It is always referred to Copley and King [1975] who reported that normal stress differences above their measurement accuracy limit of 90 mN/m^2 could not be measured.

Behaviour of blood in elongation flows

In case of low viscosity fluids as blood, stress measurements in elongation flows are extremely difficult. This explains why no report about this was found in literature.

2.3 Characteristics of the physiological flow situation

In this study the physiological flow geometry of interest is a two dimensional model of the carotid artery bifurcation, see Fig. 2.8. This geometry, as determined by Bharadvaj [1982] from 100 angiograms, is a simplification of the real three dimensional geometry. However, because of the stage of the research on this subject and the available numerical algorithms, the two dimensional model is considered as a starting point. The physiological flow is a pulse cycle. During this cycle the Reynolds number varies between 200 and 800 as is shown in Fig.

2.9 (Rindt [1989]). The time averaged mean value of this Reynolds number is 300. Rindt assumed blood to behave as a Newtonian fluid with the Reynolds number Re defined as

$$Re = \bar{u}\ \rho\ d/\eta^{\infty} \tag{2.4}$$

With $\eta^{\infty}/\rho = 3.4\ 10^{-6}$ m^2/s and D = 0.008 m (the common carotid artery diameter) this gives an average fluid velocity in the communis of 0.13 m/s. In non-Newtonian flow, this definition can be modified to (after Liepsch and Moravec [1983]):

$$Re = \bar{u}\ \rho\ d/\bar{\eta} \tag{2.5}$$

with $$\bar{\eta} = \tau(\bar{\dot{\gamma}})/\bar{\dot{\gamma}} \tag{2.6}$$

and $$\bar{\dot{\gamma}} = 2\pi\frac{\bar{u}}{d} \tag{2.7}.$$

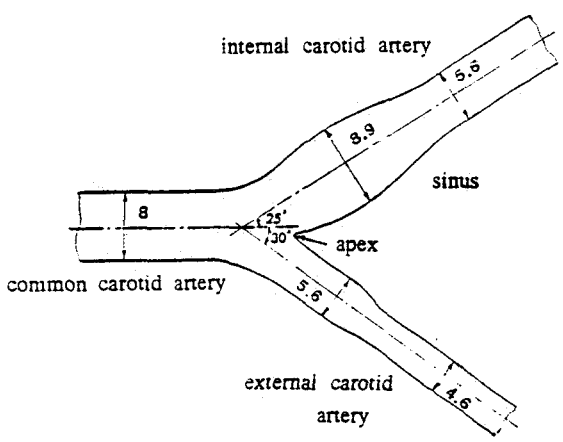

Figure 2.8 *The two dimensional model of the carotid artery bifurcation as determined by Bharadvaj (Bharadvaj [1982]).*

In viscoelastic flow, the Weisenberg number We is of importance too. It is a measure for the relative importance of viscous and elastic forces. Usually it is defined as

$$We = \frac{\lambda\bar{u}}{D} \tag{2.4}$$

with λ a characteristic relaxation time of the fluid. The data of McMillan et al [1987] (Section 2.2) suggest a characteristic relaxation time of blood as $\lambda = 0.1$ s. With this, the Weissenberg number has a value of about 1 in the physiological flow situation.

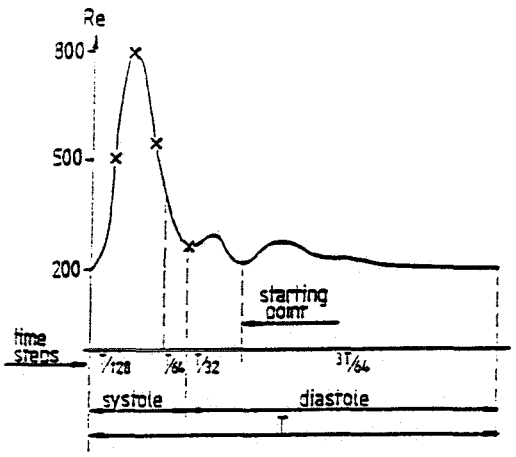

Figure 2.9 *The Reynolds number during one physiological pulse cycle according to Rindt (from Rindt [1989]).*

2.4 Constitutive models for blood

Generalized Newtonian models

In this study we will not use any generalized Newtonian model. These are very popular for describing the shear thinning effect of blood (e.g., Perktold [1989], Perktold et al [1989], Steffan et al [1989], Cho and Kensey [1991]. Some of these studies are discussed by Baaijens [1991]. They show consistently that, in order to get a more accurate flow simulation, in many cases the shear thinning character of blood should not be neglected. For several reasons however care should be taken interpreting the results of calculations with generalized Newtonian models.

First, the generalized Newtonian models are attended with some principal objections. The power-law model does not satisfy the limit situations as $\dot{\gamma}$ becomes zero or infinite, η becomes then zero or infinite. This does not agree with the experimental observations. Additionally, the value of the power n in the power-law model determines the dimension of the parameter C. This is physically unsatisfying.

In the Casson model the yield-stress is determined from measurements for small values of the shear rate. In that range the measurement accuracy is too small to ensure the yield-stress really exists.

The generalisation of 1D relations to 2D relations by using the second invariant of the

rate of deformation tensor $\mathcal{D}$ ($\dot{\gamma} = (2(\mathcal{D}:\mathcal{D}))^{\frac{1}{2}}$ is only exact in case of shear flows. This means that the derivatives must satisfy

$$\frac{\partial u}{\partial x}, \frac{\partial v}{\partial y}, \text{ and } \frac{\partial v}{\partial x} << \frac{\partial u}{\partial y}. \tag{2.4}$$

This reduces the class of possible flow problems considerably. Especially in reversed flow areas it is not ensured whether this assumption is valid.

Secondly, and more important, generalized Newtonian models are constitutive equations for visco-inelastic media. This implies that visco-elastic phenomena (Section 2.2) are ignored. However, even in steady flow convective slowing down and acceleration of the fluid occurs. The flow phenomena related with this are characterised by the Weissenberg number. In case of the physiological flow considered in Section 2.3 We=1 was found. This implies that viscoelastic effects may not be ignored a priori. Moreover, in Müller [1976] it is argued that rheological simple fluids without memory have to be lineair. Thus it can be expected that the non-lineair viscous media are having a small memory. This is in contradiction with the assumption that the medium is visco-inelastic. For this reason a generalized Newtonian constitutive equation may physically not be correct.

Extensive lists of generalized Newtonian models applied for blood are given for example by Baaijens [1991] and Cho and Kensey [1991].

Time-dependent viscoelastic constitutive models.

Several time-dependent constitutive models for blood are reported in literature. The basic mathematical equations of these models are listed in Table 2.2.
The essential similarity of all these models is their feature of having shear rate dependent parameters. In the general formulation of the Bird-Carreau equation in Table 2.2 this model differs essentially from the others by being an integral model. It can be shown that in case N_2=0 the Bird-Carreau model has an equivalent differential form too.

The Charara, Rosenblatt and Reher-Vogel models all have a constitutive equation that consists of a Maxwell type equation with time-dependent model parameters that depend on the structure by a separate structural kinetics equation.

The Rosenblatt and Reher-Vogel models are very similar, they only differ by the explicit formulation of the structural kinetics equation (the Reher-Vogel model as in Table 2.2 can easily be adjusted to the three dimensional situation by substitution of $\mathcal{T}$ for τ, $\mathcal{D}$ for $\dot{\gamma}$, and ∇ for $\dot{}$).

Table 2.2 Basic mathematical expressions of viscoelastic constitutive models proposed for blood

---

CHARARA [1985] (1 D)

"Maxwell":

$$d\tau/dt = (\dot{\gamma} - \tau/\eta_s(\omega))G_s(\omega) + \tau/G_s(\omega)\, dG_s(\omega)/dt$$

"Structure kinetics":

$$d\omega/dt = K_s(\omega)\omega[\eta_s(\omega) - \eta_s(\dot{\gamma})]^{P(\omega)}$$

ROSENBLATT [1986]

"Maxwell":

$$\lambda_{st}(P)\, \overset{\nabla}{\boldsymbol{T}}_{st}' + \boldsymbol{T}_{st}' = 2\eta_{st}(P)\boldsymbol{D}$$

"Structure kinetics":

$$dP/dt = k(1-P) - \alpha\, |\dot{\gamma}|\, P$$

REHER-VOGEL [1988] (1 D)

"Maxwell":

$$\tau + \lambda\, \dot{\tau} = (\eta(\dot{\gamma}(t),t)-\eta^{\infty})\, \dot{\gamma}$$

"Structure kinetics":

$$(\eta(\dot{\gamma}(t),t)-\eta^{\infty})+\varphi(\dot{\gamma}(t'),\dot{\gamma}(t))\partial/\partial t(\eta(I_2(t),t)-\eta^{\infty}) = \eta_e(I_2(t))$$

MODIFIED BIRD-CARREAU [1986]:

$$\boldsymbol{T} = -p\boldsymbol{I} + h \overset{0}{\underset{s=-\infty}{F}} (\boldsymbol{U}^2(x,t-s)) + 2\eta_\infty(h)\boldsymbol{D}(x,t)$$

$$\overset{0}{\underset{s=-\infty}{F}} (\boldsymbol{U}^2(x,t-s)) =$$

$$-\int_{-\infty}^{t} \underset{t'\le u\le t}{M}(t,t';\dot{\gamma}(u))[(1+\tfrac{1}{2}\varepsilon)\boldsymbol{C}^{-1}(x,t)-\tfrac{1}{2}\varepsilon\boldsymbol{C}(x,t)]dt'$$

"Structure history":

$$\underset{t'\le u\le t}{M}(t,t';\dot{\gamma}(u)) = \sum_{p\ge 1} (\eta_p/\lambda_p^2) f_p(\dot{\gamma}(t'))\exp[-\int_{t'}^{t} du/(\lambda_p g_p(\dot{\gamma}(u)))]$$

$$\tfrac{1}{2}\varepsilon = N_2/N_1$$

There are only a few calculations with the models from Table 2.2 (see references in this table). All are restricted to one dimensional, simple shear flow, and mainly concern cases with shear rates $\leq 1\ s^{-1}$. For the Reher-Vogel model no calculations were found at all.

2.5 Non-Newtonian rheological analog fluids for blood

There are several reasons to use a blood rheological analog fluid instead of blood itself: blood is unstable, tending to separate into a cell phase and a plasma phase, it is opaque to light (problematic in case of LDA measurements and flow visualization studies), it may carry disease, and it is difficult to obtain in large volumes.

In this section different fluids, which in literature are used as non-Newtonian rheological analog fluids for blood, will be discussed.

Table 2.3 lists the non-Newtonian blood rheological analog fluids used in literature with the references and a brief description of their composition given (for more information: see references). Baaijens [1991] contains a discussion about the experimental results with these fluids. The following conclusions can be made:

- Separan:
  too elastic to mimic blood accurately (see Mann and Tarbell [1989]); recently Liepsch [1991] stated that the addition of 7 - 10 % by weight DMSO (DiMethylSulphateOxide) particles reduces the elastic behaviour to adjust it to real blood.
- Milling Yellow:
  a birefringent dye that is not commercially available anymore.
- Polystyrene microspheres:
  an extremely expensive fluid when commercially obtained, and opaque for light, which makes it difficult to use in LDA experiments.
- Xanthan Gum and Xanthan Gum gel:
  according to Mann and Tarbel [1989] not accurate (too elastic).

Recently, Cho and Kensey [1991] suggested transparant slurries studied by Mannheimer [1990] might be adequate for blood too.

It is clear that no convincing rheological analog fluid exists. In some cases (Vanadium pentoxide sol, ghost cells, Separan with DMSO, "transparant slurries") there is too little experimental data available to judge the adequacy of the fluid.

Table 2.3 Non-Newtonian blood rheological analog fluids

	NAME	COMPOSITION	REFERENCES
1)	Separan	0.05 % AP30:0.04% AP45 = 3 :1 + 4% isopropanol + 0.01 % $MgCl_2$, in distilled H_20	Liepsch [1991]
2)	Milling Yellow	commercial dye in distilled H_20 ("alphanol echtgelb",Hoechst)	Schmitz [1983] Liepsch [1987]
3)	Poly-styrene micro-spheres	12 % by weight 1μm polystyrene particles in distilled H_20 + 10 mMol $CaCl_2$ + 5 % Dextran	Fukada et al [1989]
4)	Xanthan Gum	500 ppm in distilled H_20	Thurston [1989]
5)	Xanthan Gum gel	50 % by volume in glycerol	Thurston [1989]
6)	Ghost cells	washed red blood cells in distilled H_20	Liepsch et al [1991]
7)	Biconcave discs	16 % BASF particles + 2% Dextran in distilled H_20	Liepsch et al [1991]
8)	AP30	0.05 % AP30 + 4% isopropanol + 0.01 % $MgCl_2$in distilled H_20	Liepsch et al [1991]
9)	AP45	0.04 % AP45 + 4% isopropanol + 0.01 % $MgCl_2$in distilled H_20	Liepsch et al [1991]
10)	Vanadium-pentoxide sol	V_2O_5 sol in distilled H_20	Liepsch [1987]

- Ghost cells:

  there is too little experimental information about this fluid to be able to judge its appropriateness; its preparation is very complicated.

- AP30 and AP45:

  constituents of Separan fluid, Separan is a better rheological analog fluid than those two separately.

- Vanadium pentoxide sol:

  a birefringent solution that, when made in the right concentration, mimics the steady shear viscosity of blood (Liepsch [1987]). Other measurements are not known. The fluid is difficult to work with, because it becomes unstable in contact with metal or any slightest pollution.

Recently, Cho and Kensey [1991] suggested transparant slurries studied by Mannheimer [1990] might be adequate for blood too.

It is clear that no convincing rheological analog fluid exists. In some cases (Vanadium pentoxide sol, ghost cells, Separan with DMSO, "transparant slurries") there is too little experimental data available to judge the adequacy of the fluid. Many authors conclude that the microstructure of blood must be mimiced when developing a rheological analog fluid for blood.

3 Theory

3.1 Introduction

In this chapter the mathematical formulation of the Rosenblatt model is presented. No elaboration on the derivation of the model equations is given here. For that it is referred to Rosenblatt [1988].

The Rosenblatt model was chosen for the calculations because it is based on a statistical mechanics theory that relates macroscopic stresses with the micromechanics of the blood. This provides a, more or less meaningful, physical understanding. However, care must be taken with the microstructural interpretations of the model. Eventually, comparison with macroscopic experiments justify whether the model is appropriate. Initial confidence was present based on first calculations of Rosenblatt [1988] during start up and cessation of simple shear flow at shear rates of 0.05 and 1 s^{-1}. Then model predictions agreed moderately well with experimental data.

The models listed in the previous chapter in Table 2.2 do not exclude other constitutive equations from being appropriate for blood. At this stage attention is restricted to the Rosenblatt model.

As a finishing remark it is noted that the model was named "Rosenblatt model", because it was first published by Rosenblatt et al [1986] especially for blood. The resulting kinetic equation is a special case of the structural model of Liu,Soong and Williams [1984].

3.2 The Rosenblatt model

The Rosenblatt model consists of the following equations (Rosenblatt [1988]):

$$\lambda_{st} \overset{\nabla}{\boldsymbol{\tau}}_{st}' + \boldsymbol{\tau}_{st}' = 2\eta_{st}\boldsymbol{D}, \tag{3.1}$$

$$dP/dt = k(1-P)-\alpha|\dot{\gamma}| P, \tag{3.2}$$

$$\boldsymbol{\tau}' = \boldsymbol{\tau}_{st}' + (\boldsymbol{\tau}_{pl}' + \boldsymbol{\tau}_{cell}'), \tag{3.3}$$

$$\boldsymbol{\tau}_{pl}' + \boldsymbol{\tau}_{cell}' = 2\eta^{\infty}\boldsymbol{D} \tag{3.4}$$

$$\lambda_{st} = P/k, \tag{3.5}$$

$$\eta_{st} = \langle q_e^2 \rangle cP/3k, \tag{3.6}$$

$$c = wN_0\Omega/2\langle q_e\rangle, \tag{3.7}$$

$$\dot{\gamma} = (2\mathcal{D}:\mathcal{D})^{\frac{1}{2}} \tag{3.8}$$

with: $^{\nabla}$: upper convected time derivative; $\mathcal{T}$: extra-stress tensor; $\mathcal{T}_{st}$' : structure dependent (" $_{st}$ ") part of the extra stress tensor $\mathcal{T}$'; $\mathcal{T}_{pl}$': reflects the contribution of plasma viscous forces; $\mathcal{T}_{cell}$' : reflects the contribution from viscous drag between individual cells of the rouleaux and plasma; total stress tensor: $\mathcal{T} = \mathcal{T}$-p$\mathcal{I}$ (p = pressure); $\mathcal{D}$: rate of deformation tensor; $\dot{\gamma}$: shear rate; P : structure parameter, defined as the fraction of cell sides that are aggregated; λ_{st},η_{st} : structure dependent functions; α,k : model parameters; q_e: length of a rouleaux at equilibrium; $\langle q_e \rangle$ = average rouleaux length at equilibrium; N_0 : total number of (red blood) cell sides per unit volume; w : thickness of a red blood cell; Ω : spring constant in an elastic dumbbell (Hooke's law); η^∞ is the limiting steady shear viscosity at high shear rates (no structure).

The above model relates macroscopic stresses with micromechanical forces. As discussed in Chapter 2, the rheology of blood is determined by the red blood cells. Rosenblatt [1988] considers the rouleaux as primarily responsible for the time-dependent behaviour of blood. The theory is based on a statistical mechanics approach. Rouleaux are considered as Hookean elastic rods whose ensemble configuration distribution is Gaussian at equilibrium (absence of flow) and that are in affine motion (i.e., the motion at microscopic scale is equivalent with the macroscopic motion). These rouleaux are increasingly created with decreasing shear rate, while they are increasingly destructed with increasing shear rate. Orientation of particles in flow is not incorporated in this model.

Rosenblatt gave microstructural interpretations to the model parameters. The parameter α contains information primarily about cell surface chemistry. The parameter Ω, the spring constant in Hooke's law, can theoretically be calculated from k,η^0,η^∞,N_0,w, and q_e (Rosenblatt [1988], p.57). It is (Rosenblatt [1988], p. 58:) "either a measure of red cell mechanical properties or cell membrane adhesion chemistry or both, depending on which mechanism (cell-cell displacement or cell extension) is responsible for rouleau extension". Rosenblatt verified the theory by independent measurements of Ω, and found reasonable agreement with experiments.

The two basic model equations are Eqs. 3.1 and 3.2. When λ_{st} and η_{st} are constant, Eq. 3.1 simplifies to the well known upper convected Maxwell model. Eq. 3.2 reflects the competitive kinetic process of structure build-up and break down that takes place when blood is being deformed.

In this statistical mechanics theory the central concept is the aggregrate distribution function ψ in configuration space, denoted as

$$\psi(\vec{q},\vec{r},t) \qquad (3.9)$$

with $\vec{q}$ the end-to-end vector of the rouleau, $\vec{r}$ the position of the q-length rouleaux, and t the time. ψ Represents the distribution of aggregated red blood cell sides in configuration space as function of $\vec{q}$, $\vec{r}$ and t:

$\psi(\vec{q},\vec{r},t)d\vec{q}^3$ = fraction of rouleaux at time t with end-to-end vector starting on position $\vec{r}$ and the other end lying between $\vec{q}$ and $\vec{q}$ + $d\vec{q}$ (3.10).

Eq. 3.1 is derived assuming deformation of the blood satisfies the Small Strain Approximation ("SSA") (necessary to justify Hooke's law that is used to describe the elastic forces in a deforming rouleau) and assuming affine motion.

The structure kinetics equation Eq. 3.2 is derived from addition polymerization kinetics. The first term in Eq. 3.2, k(1-P), represents the *statistical* contribution to the structure kinetics. This term is derived assuming that the deformation rate is so low that only long rouleaux exist ("LRA": Long Rouleaux Approximation). If we write k(1-P) = k - kP, k represents the *formation* of q-length aggregates by combination of shorter rouleaux, and -kP represents the *loss* of q-length rouleaux by combination with any other length rouleaux.

The second term in Eq. 3.2, $-\alpha|\dot{\gamma}|P$, represents the *hydrodynamic* contribution to the structure kinetics process. It reflects the *loss* of q-length rouleaux by shearing forces.

For calculating stresses in shear flows, Rosenblatt [1988] fitted the model to data measured in the limiting low shear rate range ($\dot{\gamma} < 10\ s^{-1}$).

The addition of this retardation term $2\eta^{\infty}D$ yields a constitutive equation that does not satisfy the postulates of Simple Fluid theory, because step strains, i.e., infinite strain rates, are not possible without infinite stresses. This deficiency is accepted, because in some respects the model will appear to be very realistic (see Chapt. 4).

At very low steady shear rates (P = 1) the shear viscosity η equals η^0. From Eqs. 3.3 - 3.7 then follows $\eta_{st}^{0\prime} = (\eta^0 - \eta^{\infty})$ P (and $\eta_{st}^{0\prime} = \langle q_e \rangle w N_0 \Omega / 6k$ ($\langle q_e \rangle^2 \simeq \langle q_e^2 \rangle$)).

Essentially, the model contains four model parameters: η^0, η^{∞}, α, and k. From fits on measured shear stresses of blood after shear rate steps form 0 to $\dot{\gamma}$ = 0.05 and 1 s^{-1}, during thixotropic loops (a to a maximum of 2 s^{-1} linearly with time increasing shear rate and decreasing back to 0 s^{-1} again), Rosenblatt [1988] found as numeric values: η^0 = 0.12 Pa s, η^{∞} = 0.004 Pa s, α = 1.2, k = 0.25 s^{-1}.

At this stage of this research, primarily the macroscopic predictions of the model are

investigated. Although the Rosenblatt model is based on the assumption of low deformations and deformation rates, in this study the model will be used in other situations too. Then, its micromechanic background cannot be hold anymore. Other mechanisms such as deformation, orientation, and collision of the red blood cells are responsible for the viscoelastic behaviour of blood too. The parameter P cannot be interpreted anymore as "the fraction of red cells that is aggregated", but it must be seen as a mathematical parameter.

3.3 Generalisation to multi mode

The Rosenblatt model can be generalized to a N mode version in the following trivial way.

$$\lambda_{st_i} \overset{\nabla}{\boldsymbol{\tau}}_{st_i}' + \boldsymbol{\tau}_{st_i}' = 2\eta_{st_i}\boldsymbol{\mathcal{D}}, \tag{3.9}$$

$$dP_i/dt = k_i(1-P_i) - \alpha_i |\dot{\gamma}| P_i, \tag{3.10}$$

$$\boldsymbol{\tau}' = \sum_i^N \boldsymbol{\tau}_{st_i}' + (\boldsymbol{\tau}_{pl}' + \boldsymbol{\tau}_{cell}') \tag{3.11}$$

$$\boldsymbol{\tau}_{pl}' + \boldsymbol{\tau}_{cell}' = 2\eta^{\infty}\boldsymbol{\mathcal{D}} \tag{3.12}$$

$$\lambda_{st_i} = P_i/k_i \tag{3.13}$$

$$\eta_{st_i} = \eta_{0i} P_i \tag{3.14}$$

These equations have not been derived from micromechanic considerations. It is proposed as a mathematical generalisation of the single mode model. However, this formulation implies some assumptions. For example, the structure kinetics equations (3.10) are considered to be independent (there is no relation between different P_i's). Hence, different structural processes are not allowed to interfere. Here, we do not speculate what kind of processes these are. Without physical evidence, it is assumed that all processes can be described by the same structure kinetics equation that was originally set up to describe the aggregation of red blood cells at low deformation rates. Therefore the parameters P_i cannot be regarded as "the fraction of cells that is aggregated", but must be considered as a mathematical parameter.

4 Calculations in simple shear flow

4.1 Introduction

Simple shear flow belongs to the class of viscometric flows. Viscometric flows enable to characterize material behaviour of fluids. In simple shear flow, shear stress measurements are relatively easy to perform. These experiments are very useful to identify parameters in constitutive models.

In case of the Rosenblatt constitutive model it is shown in this chapter that all model parameters can be obtained from fits on shear stress measurements in simple shear flow (Sections 4.2 - 4.4). Both calculated shear and normal stresses in unsteady simple shear flow (in start up, cessation of, and small amplitude sinusoïdally flow) are compared with experimental data of blood found in literature. Finally, the multi mode version of the model is discussed (Section 4.5).

The main conclusion is that the Rosenblatt model can describe well the shear stresses in start up of steady shear flow for shear rates of magnitude 10 - 30 s^{-1} (no experimental data were available for higher shear rates). The first normal stress difference was less than the measurement accuracy (90 mPa) of Copley and King [1975], who could not measure any normal stress difference significantly different from the measurement error (see Section 2.2). Hence, the model calculations at least do not contradict the available experimental data with respect to the normal stress differences.

4.2 Parameter identification for the Rosenblatt model

In simple shear flow, the equations for the structure dependent part of the Rosenblatt model as defined in Chapt. 3, read:

$$\lambda \frac{d}{dt}(\tau_{xx,st}') + \tau_{xx,st}' - 2\lambda\dot{\gamma}\tau_{xy,st}' = 0 \tag{4.1}$$

$$\lambda \frac{d}{dt}(\tau_{xy,st}') + \tau_{xy,st}' = \eta\dot{\gamma} \tag{4.2}$$

$$\tau_{yx,st}' = \tau_{xy,st}' \tag{4.3}$$

$$\tau_{yy,st}' = 0 \tag{4.4}$$

$$\eta = \eta^0 P \tag{4.5}$$

$$\lambda = P/k \tag{4.6}$$

$$dP/dt = k - (k + \alpha|\dot{\gamma}|)P \tag{4.7}$$

$$\tau_{xy}' = \tau_{xy,st}' + \eta^{\infty}\dot{\gamma} \tag{4.8}.$$

All other stress components ($\tau_{xz},\tau_{zx},\tau_{yz},\tau_{zy},\tau_{zz}$) are zero. These equations contain four independent model parameters: k,α,η^0,and η^{∞}. In simple shear flow, only measurements of τ_{xy} have been reported (see also Chapt. 1). All fitting in this chapter is based on Eq. 4.8.

Steady simple shear

-Shear viscosity

The parameters $\alpha/k,\eta^0$,and η^{∞} can be obtained by fitting the steady shear viscosity. In steady simple shear, the shear viscosity η is given by

$$\eta = (\eta^0-\eta^{\infty})/(1+(\frac{\alpha}{k}|\dot{\gamma}|) + \eta^{\infty} \tag{4.9}.$$

This equation contains the four unknown model parameters. For fitting equation (4.9) we have used the steady shear viscosity of human blood measured by McMillan et al [1987]. From these data, we obain $\eta^0 = 0.12$ Pa s and $\eta^{\infty} = 0.0037$ Pa s.

The parameter $\frac{\alpha}{k}$ was determined using a non-linear least squares method based on a Newton-Raphson method (Press et al [1987], Chapt. 14). The result was $\frac{\alpha}{k} = 9.1$ s.

Rosenblatt [1988] fitted this model by visual comparisons of model predictions with experimental shear stress data. He obtained parameters η^0 and η^{∞} as described above (0.12 Pa and 0.004 Pa s respectively) from a steady shear viscosity fit on experimental data of Huang et al [1973]. To find values for α and k, he first estimated reasonable ranges of α and k from a comparison of stress growth data with model predictions (after a shear rate step from 0 to 0.05 and to 1 s^{-1}). The best fit parameters were then determined from visual comparisons of model predictions with experimental data in two shear rate hysteresis experiments (a shear rate loading program with shear rate increasing linearly in time from 0 to a maximum and then symmetrically decreasing to 0 again). Two cases were considered: one with a maximum shear rate of 0.12 s^{-1} and one with a maximum of 1 s^{-1}, yielding parameter values $\alpha = 1.2$ and k =

0.25 s^{-1}, thus $\frac{\alpha}{k}$ = 4.8 s.

The difference between the values of the two parameter sets and their predicted stresses is rather large. Fig. 4.1 shows the steady shear viscosity for both parameter sets together with experimental data of McMillan et al. [1987]. The two parameter sets yield significant different steady shear viscosity curves. It appears that ath the higher shear rates the parameter set of Rosenblatt et al [1987] is more accurate compared with ours. Because of their larger magnitude, measured steady shear viscosities at shear rates below 1 s^{-1} dominated our steady shear viscosity fit from which we determined $\frac{\alpha}{k}$. Apparently, the one mode model is not adequate, more modes are necessary (see Section 4.4).

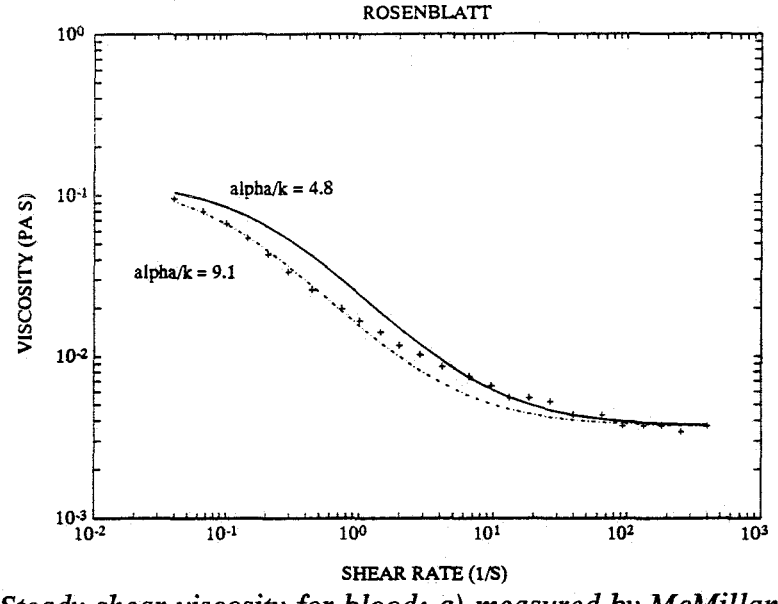

Figure 4.1 *Steady shear viscosity for blood: a) measured by McMillan et al [1987] (+), b) model curve for the Rosenblatt model with fitted parameters of Rosenblatt [1988] (–), and c) "best" fit in a least square sense (-·).*

- Normal stresses

The Rosenblatt model also predicts the normal stres τ_{xx} in steady shear flow. In literature, no succesfull normal stress measurements distinguishable from measurement errors are reported for blood (Copley and King [1975]). Their (large) measurement error was 90 mPa.

In steady simple shear, the model predicts:

$$\tau_{xx} = 2(\frac{1}{k})\eta_0\dot{\gamma}^2(1+(\frac{\alpha}{k})|\dot{\gamma}|)^2 \qquad (4.10).$$

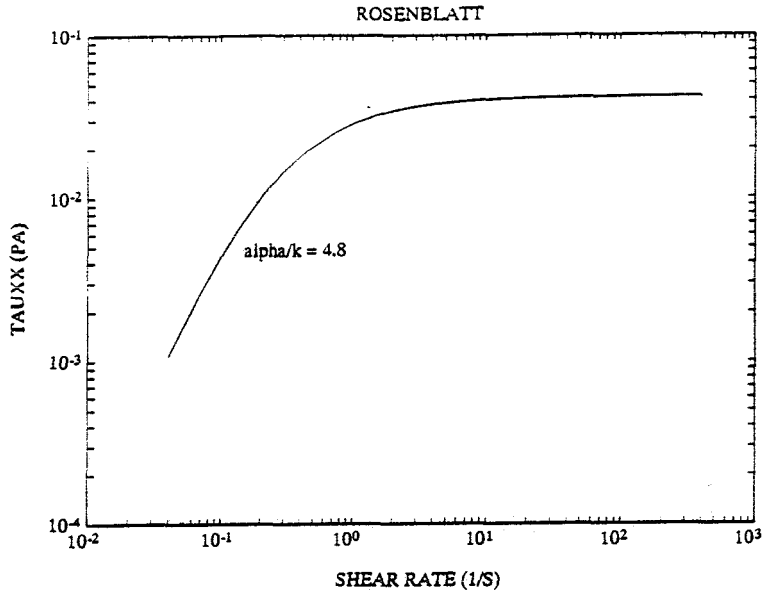

Figure 4.2 *Normal stress τ_{xx} as a function of steady shear rate for the set with α = 1.2 and k = 0.25 s^{-1}.*

For the limit $(\frac{\alpha}{k})|\dot{\gamma}| >> 1$ (at high shear rates) τ_{xx} reaches a constant value that is also the maximum value:

$$\tau_{xx} = 2\eta^0/((\frac{\alpha}{k})\alpha) \qquad (4.11).$$

If we demand the normal stresses to have a certain maximum value Max, using $\frac{\alpha}{k}$ = V the condition

$$\alpha \geq 2\eta^0/(\text{V Max}) \qquad (4.13)$$

follows. In case of a maximum for τ_{xx} of 90 mPa (the measurement error), with the values $\frac{\alpha}{k}$ = 4.8 s and 9.1 s the constraints $\alpha \geq 0.55$ and $\alpha \geq 0.29$ are found respectively. In case of $\frac{\alpha}{k}$ = 9.1 the values of α and k have not been determined separately. In the following, only the parameter set α = 1.2 and k = 0.25 s^{-1} is used. The reason for this is the fact that the available experimental data in unsteady simple shear flows that we are interested in is measured in the shear rate interval 8 - 30 s^{-1} (Section 4.3), in which the set α = 1.2 and k = 0.25 s^{-1} gives the best agreement between steady shear viscosity data measured on human blood and model predictions. The set satisfies also $\alpha \geq 0.29$.

4.3 Response after shear rate steps in simple shear

- Shear stresses

Having determined the model parameters for the Rosenblatt model as described in the previous section, stress response in several start up of steady simple shear flow experiments was calculated. The results are compared with experimental data of blood reported by McMillan et al [1987].

Three different simple shear experiments are considered whereby during two separate periods of time a constant shear rate is applied. The constant shear rates are 8, 13, and 30 s^{-1} respectively. Stress measurements during such an experiment cover several phenomena: stress growth (after a shear rate step from rest to a steady value), stress relaxation (after a shear rate step from a steady value to zero), and influence of shear history (the difference between the response after the second step compared with the first).

The stress responses were numerically calculated from Eqs. 4.1 - 4.8. A backward Euler difference scheme was used to avoid possible numerical difficulties caused by the stiffness of the differential equations. The parameter set α = 1.2, k = 0.25 s^{-1} was used, with 1000 time points (accuracy of the solution was checked by doubling this number), and a ramp of 0.075 s during each shear rate step, to mimic the experimental conditions of McMillan et al [1987].

The model parameters as determined by Rosenblatt et al [1987] give very good results in all three cases. This is illustrated in Fig. 4.3 in case of a single shear rate step from 0 to 8 s^{-1}.

From Fig. 4.3 a) - c) it is concluded that the Rosenblatt model with α = 1.2 and k = 0.25 s^{-1} describes shear stresses well during stress growth, stress relaxation, and steady shearing in these three cases. Just like the measured data, the model calculations show the typical stress overshoot. The largest differences between calculations and measurements are found in this stress overshoot peak. Duration in time of the calculated peak agrees well with measurements, but the maximum heigth of the calculated peak is reached approximately 0.2 s in time later compared with experiments.

The maximum overshoot peak heigth in the calculations displayed in Figs. 4.3 a) and b) is also approximately 10 % heigher compared with measured data. In case of Fig. 4.3 c) (shear rate step to $\dot{\gamma}$ = 30 s^{-1}) the maximum overshoot peak heigth agrees well with the measured data (difference < 1%). In this latter case, the stress relaxation after cessation of shearing is described less accurate than in Figs. 4.3 a) and b).

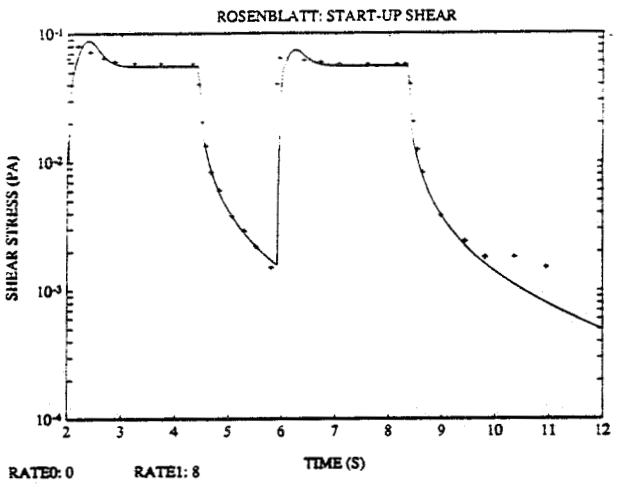

a) $\dot{\gamma} = 8\ s^{-1}$

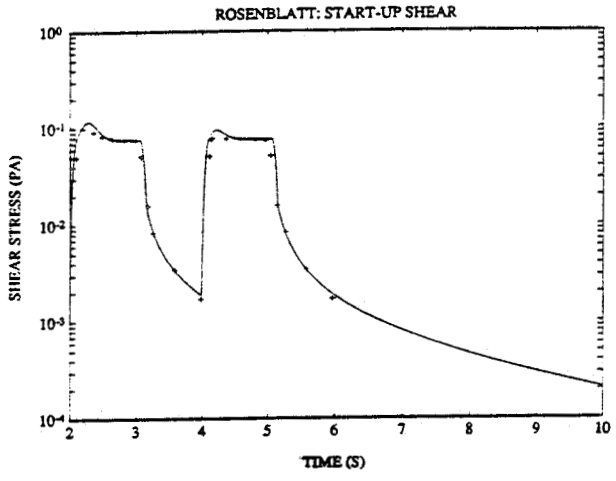

b) $\dot{\gamma} = 13\ s^{-1}$

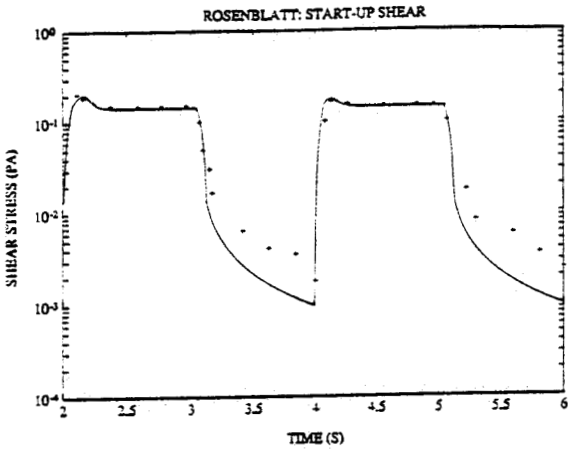

c) $\dot{\gamma} = 30\ s^{-1}$

Figure 4.3 *Shear stress responses during simple shearing whereby during two periods of time, separated by a non shearing period, a constant shear rate is applied. The curves are calculated using $\alpha = 1.2$ and $k = 0.25\ s^{-1}$. At each rate step a ramp of 0.075 s was used. Measured data (+) are from McMillan et al [1987].*

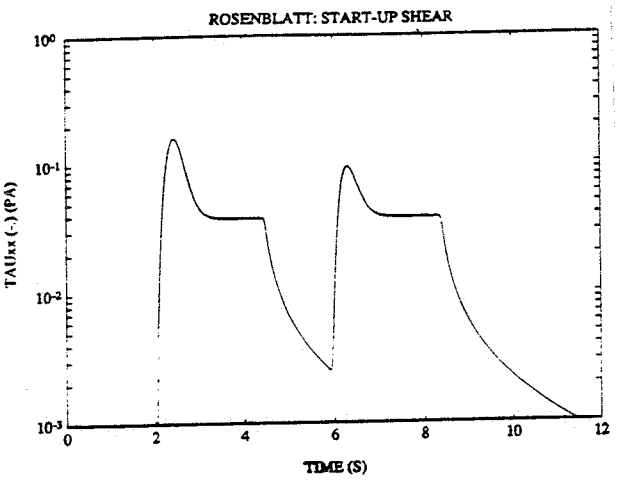

a) $\dot{\gamma} = 8\ s^{-1}$

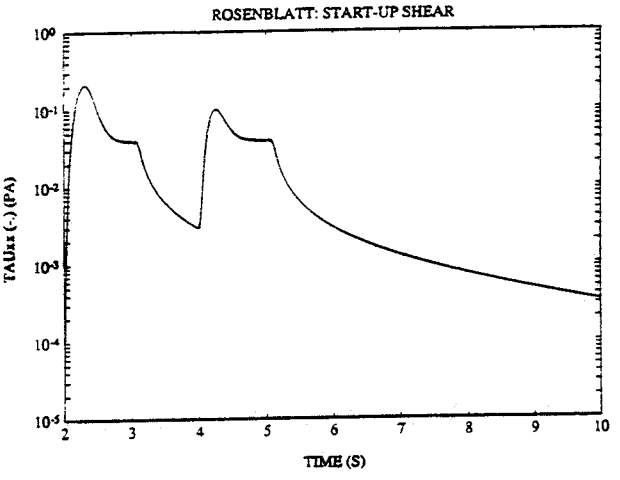

b) $\dot{\gamma} = 13\ s^{-1}$

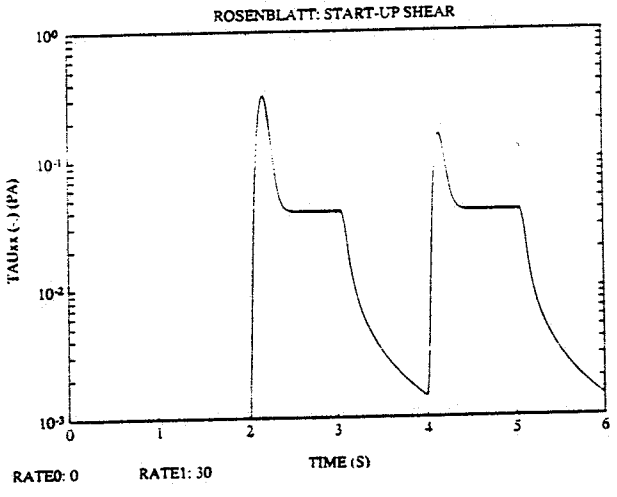

c) $\dot{\gamma} = 30\ s^{-1}$

Figure 4.4 *Response of normal stress τ_{xx} during three simple shearing experiments (same as Figure 4.3) whereby during two periods of time, separated by a non-Newtonian shear period, a constant shear rate is applied. Curves are calculated using $\alpha = 1.2$ and $k = 0.25\ s^{-1}$. At each rate step a ramp of 0.075 s was used.*

- Normal stresses

The parameter set used yields a normal stress τ_{xx} that is smaller than the measurement accuracy of the experiments of Copley and King [1975]. Steady state values for τ_{xx} were already shown in Fig. 4.2. After a shear rate step also the normal stresses τ_{xx} has an overshoot peak.

4.4 Complex viscosity

The Rosenblatt model can also describe complex viscosity measurements. In fact, the structure dependent Eq. 3.1 then changes into the ordinary linear Maxwell model. This can be understood as follows. The complex viscosity is defined in small amplitude sinusoïdally shear flow under the condition that the stress τ depends linearly on γ. In general the Rosenblatt model is a non-linear model: applying a small strain oscillatory simple shear flow $\gamma = \gamma_0 \exp(i\omega t)$ does not yield a linear response in τ. This follows immediately from substitution of the expression for γ in Eq. 3.1.

The non-linearity is caused by the time-dependency of the parameters η and λ in Eq. 3.1. These are calculated from the structure kinetics equation (Eq.3.2). The model is linear if and only if the parameters η and λ (and consequently P) are constant in time. This is the case during oscillating shear when P = 1. The model then changes into the linear Maxwell model. If the structure kinetics equation is written as

$$dP/dt = k - P(k + \alpha|\dot{\gamma}|) \qquad (4.14)$$

the condition P = 1 is obviously met if and only if

$$\alpha|\dot{\gamma}| << k \qquad (4.15).$$

Condition 4.15 implies that the Rosenblatt model violates one of the principle of simple fluid theory, that states that no matter how high the oscillation frequency is, as long as the strain amplitude is small enough, the stress response will be linear. Eq. 4.15 can be written as $\alpha|\gamma\omega| << k$. This means that the strain amplitude below which the response is linear depends on the (angular) frequency (see also Larson [1988], p. 179).

Multi modes are necessary to fit the Rosenblatt model on measurements of the complex viscosity blood reported by Thurston [1979]. In case of a multi mode linear Maxwell model the viscous (η') and elastic (η'') components of complex viscosity are described by (e.g. Tanner [1985])

$$\eta' = \sum_i \eta_{0i}/(1+\omega^2\lambda_{0i}^2) \quad (4.16),$$

$$\eta'' = \sum_i \omega\, \eta_{0i}\, \lambda_{0i}/(1+\omega^2\lambda_{0i}^2) \quad (4.17).$$

In case of the Rosenblatt model, the component η' is given by

$$\eta' = \sum_i \eta_{0i}\, \lambda_{0i}/(1+\omega^2\lambda_{0i}^2) + \eta^\infty \quad (4.18).$$

We found 5 modes to be sufficient for fitting experimental data. First, the time constants λ_{0i} were chosen, which results in a linear set of equations. With this set the zero shear viscosities η_i were fitted with an ordinary least squares routine (minimizing both $\| \eta'-\eta'_{exp} \|_2$ and $\| \eta''-\eta''_{exp} \|_2$). When $\omega \to 0$ rad/s also $\dot\gamma \to 0$ s^{-1}, thus $\eta'' \to 0$ Pa s and $\eta' \to \sum_i \eta_{0i} = \eta^0-\eta^\infty$. The condition $\sum_i \eta_{0i} = \eta^0-\eta^\infty$ was added to the system of equations. Fig. 4.5 shows the result.

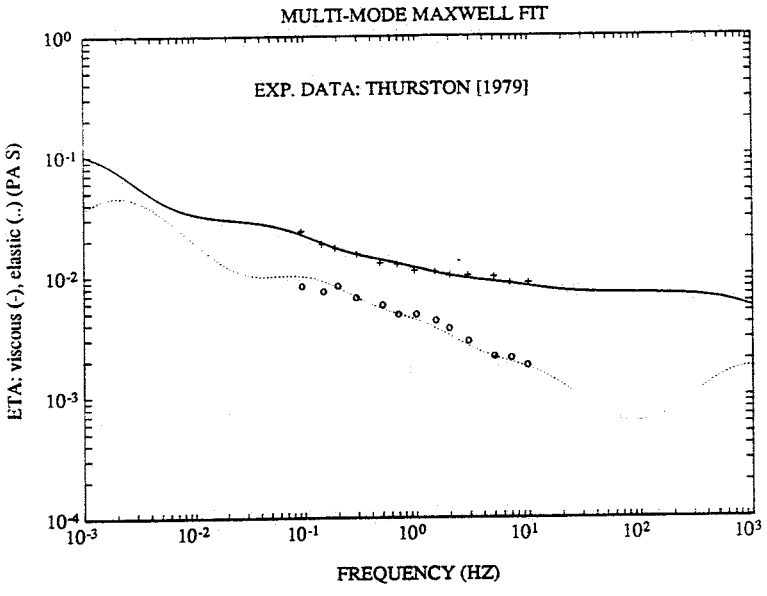

Figure 4.5 *5-Mode linear Maxwell model fitted on measurements of the complex viscosity of blood (Thurston [1979]): (+) measured η', (o) measured η'', (-) fitted η', (· ·) fitted η''.*

Although the fit of the complex viscosity agrees well with the measured data of both η' and η'', outside the (small) measurement interval the fit has oscillations that are expected to be unrealistic. Unfortunately the measurements cover only the small frequency range between 0.10 and 10 Hz. The fit was made in order to get curves as smooth as possible. A very large time constant (λ_{01} = 500 s) was necessary to fit the model as best as possible on the experimental data. However, from a physical point of view, 500 s is a very large relaxation time for a low viscosity fluid like blood. Extrapolation of the fit outside the frequency interval of the measured data is not allowed. To obtain a much more reliable fit, experimental data of the complex viscosity in a larger frequency interval (for example: a logarithmic range from 0.001 to 1000 Hz) and more modes are necessary.

The parameters η_{0i} and λ_{0i} obtained in this way are listed in Table 4.1 in the next section.

4.5 Multi mode Rosenblatt model

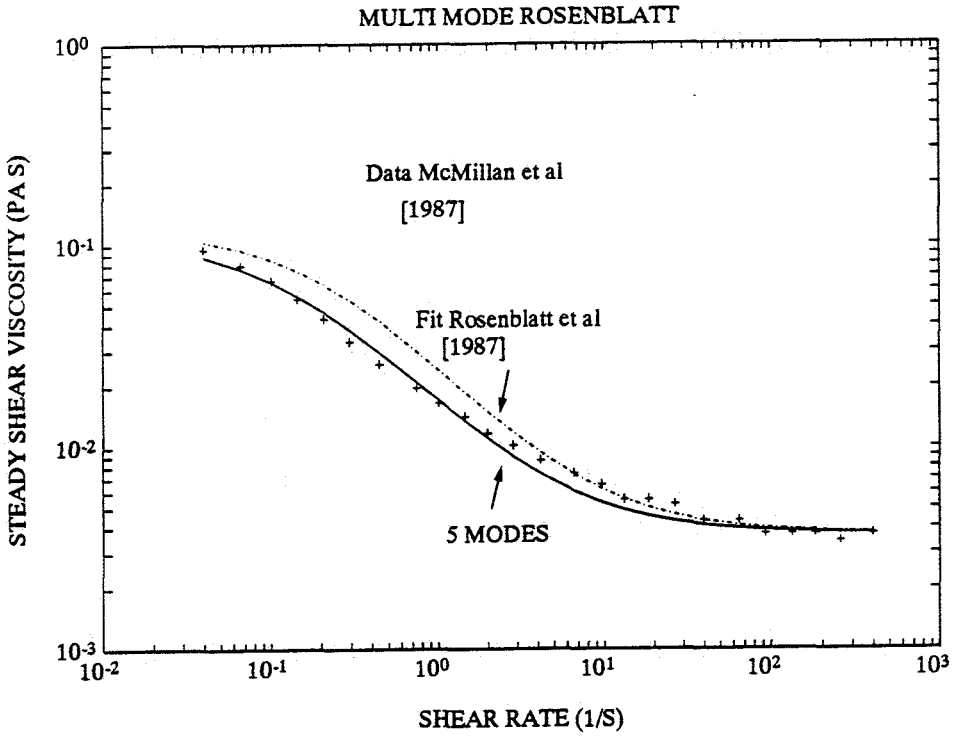

Figure 4.6 *Steady shear viscosity of blood: (+) measured (Thurston [1979]), (-) 5-mode Rosenblatt model with parameters as in Table 4.1, (-·) single mode fit with α = 1.2 and k = 0.25 s^{-1}.*

The complex viscosity fit in Fig. 4.5 enables to identify the parameters k_i from the parameters λ_{0i} for a multi-mode Rosenblatt model, because $k_i = 1/\lambda_{0i}$. The remaining parameters α_i can be obtained by fitting the model equation for the steady shear viscosity on experimental data.

The steady shear viscosity η is now given by

$$\eta = \sum_i \eta_i + \eta^{\infty} \tag{4.19}$$

with η_i for a single mode given by

$$\eta_i = \eta_{0i}/(1+(\frac{\alpha}{k_i})|\dot{\gamma}|) \tag{4.20}.$$

Eq. 4.19 is non-linear in α_i, therefore we used the non-linear least squares method in Press et al [1987] (Chapt. 14). Fig. 4.6 presents the result together with the single mode fit of Rosenblatt [1988] (α = 1.2, k = 0.25 s^{-1}). Comparing this with the single mode case in Fig. 4.1 the multi mode model evidently improves the fit significantly.

Table 4.1

5 Mode Rosenblatt model parameters for blood *)

i	λ_{0i}	η_{0i}	α_i
1	500	0.0905	0.0224
2	10	0.0154	0.4886
3	1	0.0048	5.4159
4	0.1	0.0021	1.2218
5	0.001	0.0034	400.55

*) Fitted on experimental data for η^* of Thurston [1979].

The contribution to the steady shear viscosity of each mode separately is drawn in Fig. 4.7 together with the summed result and experimental data of McMillan et al [1987] (actually

η-η^{∞} is plotted).

For each mode, the end value of the normal stress τ_{xx} in steady simple shear can be calculated (using Eq. 4.11). Results are given in Table 4.2.

Table 4.2

Limit values of normal stresses τ_{xx} at high shear rates in steady simple shear modes of the 5-mode Rosenblatt model	$\tau_{xx,i}$ (Pa)
	0.7193
	0.0129
	0.0003
	0.0282
	4.26 10-5

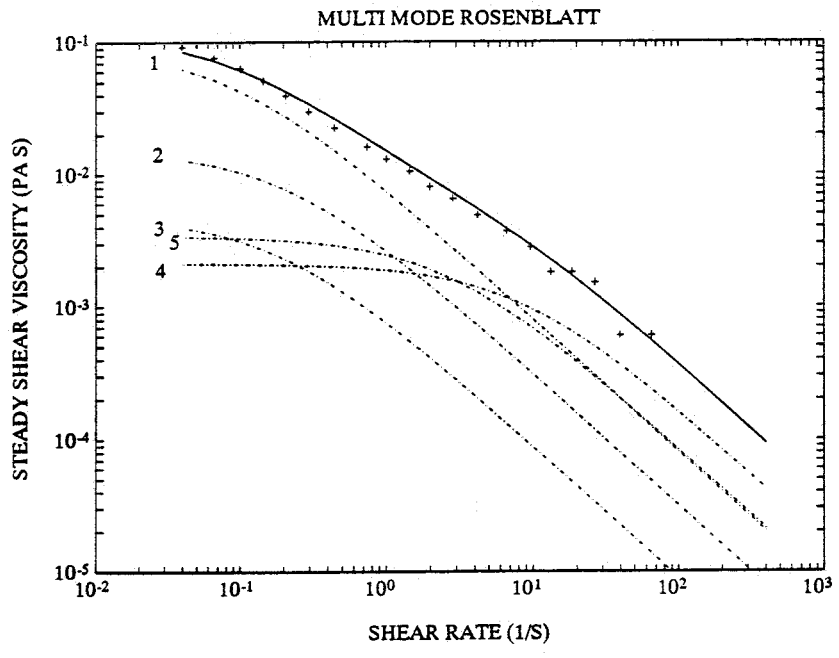

Figure 4.7 *Steady shear viscosity (η-η^{∞}) of blood: (+) measured (Thurston [1979]), (-) separate modes of the 5-mode Rosenblatt model with parameters as in Table 4.1.*

Because $\tau_{xx,1}$ > 90 mPa, it is clear that the first mode, has an unrealistically high normal stress. The other $\tau_{xx,i}$ are smaller than 90 mPa. The sum of all $\tau_{xx,i}$ is 0.76, which is much to large (≈ factor 10). We return to the multi mode model in Chapter 5.

4.6 Conclusions

In comparison with experimental data for blood reported by McMillan et al [1987], the model parameter set with α = 1.2 and k = 0.25 s^{-1} yields accurate shear stresses in steady, start up and cessation of simple shearing with $\dot{\gamma}$ = 8, 13 and 30 s^{-1}.

It predicts also normal stresses τ_{xx} smaller than the measurement accuracy of normal stress measurements of blood reported by Copley and King.

In case of the multi mode version of the Rosenblatt model, the model parameters k_i and η_i can be obtained from fits on measurements of the complex viscosity and the steady shear viscosity. However, more experiments in a broader frequency range are necessary to improve the fit over a broader frequency range. Measurements of the complex viscosity of blood should be available in a much broader frequency interval (for example 6 decades).

Compared with the single mode model, the fit of the steady shear viscosity is improved significantly by the 5-mode version.

The 5 mode model predicts a too high normal stress τ_{xx} in steady simple shear flow at high shear rates. This is caused by the first mode with λ = 500 s, which is a very large relaxation time for blood from a physical point of view.

Remarkably, although the Rosenblatt model was originally derived assuming small deformation rates with $\dot{\gamma} \leq 1$ s^{-1} ("Long Rouleaux Approximation", Chapt. 3), the model describes also unsteady shear flows well with shear rates of magnitude 8 - 30 s^{-1}. This implies that care should be taken with microstructural interpretations of the Rosenblatt model, at least when $\dot{\gamma} \geq 1$ s^{-1}.

The Rosenblatt model violates one of the principles of simple fluid theory, because its response changes into linear viscoelastic response depending on the shear rate, instead of on shear strain only.

5 Calculations in simple elongational flow

5.1 Introduction

In literature, no experimental data with regard to elongational flow of blood are reported. Measurements of elongational viscosity are extremely difficult in case of low viscosity fluids such as blood. It is expected that blood is at most only slightly sensitive for elongational deformation. Nevertheless it is important to study the behaviour of the constitutive model in such flows. The constitutive model might cause unrealistic phenomena in flow simulations of blood when it predicts strong effects in elongational deformation.

First, steady simple elongation is considered (Section 4.2), then start up of simple elongation is discussed (Section 4.3). Conclusions are made in Section 4.4.

The dataset with $\alpha = 1.2$ and $k = 0.25\ s^{-1}$ is used. Results show that if the elongation rate step is larger than $1\ s^{-1}$ the Rosenblatt model predicts relatively high elongational viscosities in start up of simple elongation. No calculations with the 5 mode model were made, because the first mode showed a singularity in the elongational viscosity.

5.2 Steady simple elongation

The Rosenblatt model equations in steady simple elongation are:

$$\tau_{xx} = 2G\dot{\varepsilon}/(k + (\alpha\sqrt{3} - 2)|\dot{\varepsilon}|) \tag{5.1}$$

$$\tau_{yy} = -G\dot{\varepsilon}/(k + (1 + \alpha\sqrt{3})|\dot{\varepsilon}|) \tag{5.2}$$

$$G = \eta/\lambda \tag{5.3}$$
$$\eta = \eta^0 P^0 \tag{5.4}$$
$$\lambda = P^0/k \tag{5.5}$$
$$P^0 = k/(k + \alpha\sqrt{3}|\dot{\varepsilon}|) \tag{5.6}$$

Hence the elongational viscosity is given by

$$\bar{\eta} = (\tau_{xx} - \tau_{yy})/\dot{\varepsilon} \tag{5.7 a}$$
$$= 2G/(k + (\alpha\sqrt{3} - 2)|\dot{\varepsilon}|) + G/(k + (1 + \alpha\sqrt{3})|\dot{\varepsilon}|) \tag{5.7 b}$$

Eq. 5.7b, with $\eta^0 = 0.12$ Pa, $\alpha = 1.2$ and $k = 0.25\ s^{-1}$ (see Chapt. 4), is plotted in Fig. 5.1 together with the shear viscosity as function of deformation rate (= elongation rate or shear

rate). A third variable is also plotted: the Trouton ratio that equals the elongational viscosity divided by the shear viscosity. For a Newtonian fluid this ratio is equal to 3. In Fig. 5.1 this ratio first equals 3 at deformation rates below 0.1 s^{-1}, and then it increases to a maximum value of about 10 at a deformation rate of 5 s^{-1}. At higher deformation rates, the Trouton ratio decreases continuously. The minimum value displayed is 0.2 at a deformation rate of 1000 s^{-1}. Hence in steady simple elongational flow the elongational viscosity is not very large compared with the shear viscosity in steady simple shearing.

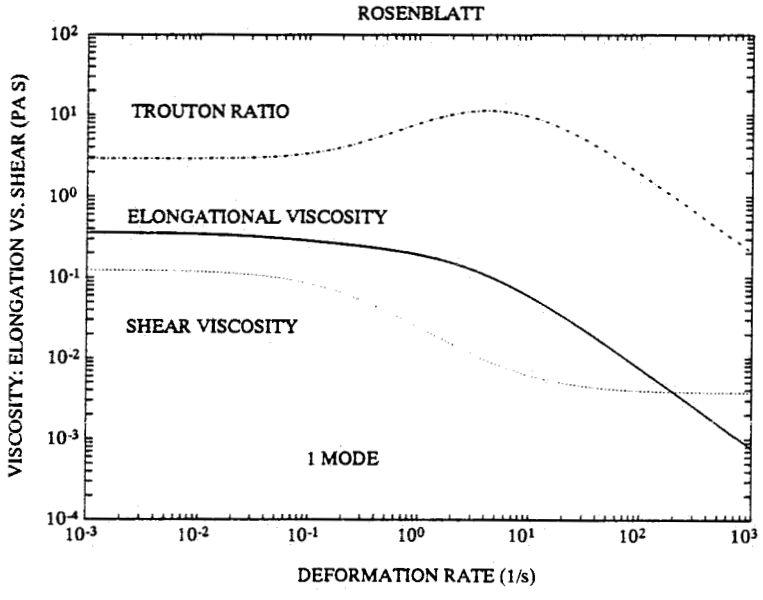

Figure 5.1 *Steady elongational viscosity (——), steady shear viscosity (· · ·), Trouton ratio (–·) in case of the Rosenblatt model with α = 1.2 and k = 0.25 s^{-1}.*

Notice from Eq. 5.7b that the elongational viscosity can have a singularity. This is the case when $(\alpha\sqrt{3} - 2) < 0$ (then for $\dot{\varepsilon} = -k/(\alpha\sqrt{3} - 2)$ the first term in Eq. 5.7b goes to infinity). This can be avoided by enforcing as constraint on α $(\alpha\sqrt{3} - 2) > 0$, thus $\alpha > 2/\sqrt{3}$ (= 1.15) when fitting the steady shear viscosity. In case of the single mode model both parameter sets, obtained from simple shear experiments (Section 4.2), satisfy this constraint. In the multi mode case this is not the case for all modes (see Table 4.2).

The parameters α_i for the multi mode version are obtained by fitting the steady shear viscosity (Section 4.5). When fitting the steady shear viscosity, with the 5-mode model satisfying constraints $\alpha_i > 2/\sqrt{3}$, this did not give an acceptable result. These constraints were

enforced by substitution of $\alpha_i = (\beta_i + 2)/\sqrt{3}$ and using the non-negative Least Squares method described in Lawson and Hanson [1974]. The fit was worse than the single mode fit, and, compared with the measured steady shear viscosity, much too large to be acceptable.

This can be explained as follows. The large deviation is caused by the first mode with $\lambda_1 = 500$ s, that mainly determines the fit (see Section 4.5). The contribution of each mode to the steady shear viscosity is given by $\eta_{0i}/(1+|\dot\gamma|(\beta_i+2)/k_i\sqrt{3})$. For small shear rates this expression equals η_i, for large shear rates it goes to $\eta_{0i}/(|\dot\gamma|(\beta_i+2)/(k_i\sqrt{3}))$, a continuous descending straigth line on a log-log plot of the viscosity versus shear rate. The transition between the two limits takes place at the "transition shear rate" $|\dot\gamma|_{tr} = k_i\sqrt{3}/(\beta_i+2) = \sqrt{3}/(\lambda_{0i}(\beta_i+2))$. In case of $\lambda_{01} = 500$ s this term equals $\sqrt{3}/(500(\beta_i+2))$. If $\beta_i = 0$ ($\alpha_i = 2/\sqrt{3}$) then $|\dot\gamma|_{tr} \approx 0.001$. Any $\beta_i > 0$ ($\alpha_i > 2/\sqrt{3}$) gives a smaller value for $|\dot\gamma|_{tr}$, making the fit worse. In this respect too, $\lambda_1 = 500$ s is a bad choice. Apparently, to obtain a good fit of the multi mode model, constraints must be enforced on the time constants λ too. More important is the need for measurements of the complex viscosity of blood in a broader frequency interval ($0.001 < f < 1000$ Hz), as it was concluded already in Chap. 4.

5.3 Start up of simple elongational flow

Some constitutive models predict a very large maximum in the elongational viscosity during start up of simple elongational flow (i.e., an elongational rate step from zero to a steady value). This is not expected to be the case for human blood, because of its relatively small elongational viscosities.

The elongational viscosity is still defined by relation (5.7 a). All stress tensor components follow from Eqs. 5.8 - 5.15:

$$\frac{d\tau_{xx}'}{dt} + (\tfrac{1}{\lambda} - 2\dot\varepsilon)\tau_{xx}' = 2\eta\dot\varepsilon\tfrac{1}{\lambda} \qquad (5.8)$$

$$\frac{d\tau_{yy}'}{dt} + (\tfrac{1}{\lambda} + \dot\varepsilon)\tau_{yy}' = -\eta\dot\varepsilon\tfrac{1}{\lambda} \qquad (5.9)$$

$$\tau_{xy}' = \tau_{yx}' = \eta_\infty\dot\gamma \qquad (5.10)$$

$$\tau_{zz}' = \tau_{yy}' \qquad (5.11)$$

$$\eta = \eta^0 P \qquad (5.12)$$

$$\lambda = P/k \qquad (5.13)$$

$$dP/dt = k - (k+\alpha|\dot\gamma|)P \qquad (5.14)$$

$$\dot\gamma = (2\,\boldsymbol{D}\cdot\boldsymbol{D})^{\frac{1}{2}} = \sqrt{3}|\dot\varepsilon| \qquad (5.15).$$

This system of equations has been solved using a backwards differential Euler scheme. In Fig. 5.2, 6 calculations are presented for elongational rate steps from zero to 0.1, 0.25, 0.50, 1, 2, 5 s^{-1}. All calculations have been performed using a ramp of 0.075 s as in Chapt.3 in case of start up of simple shear, and using 1000 time discretisation points (only in case of the rate step to 0.1 s^{-1} 2000 points were used). Accuracy of the solution was checked by doubling the number of time discretisation points, which did not influence the solution.

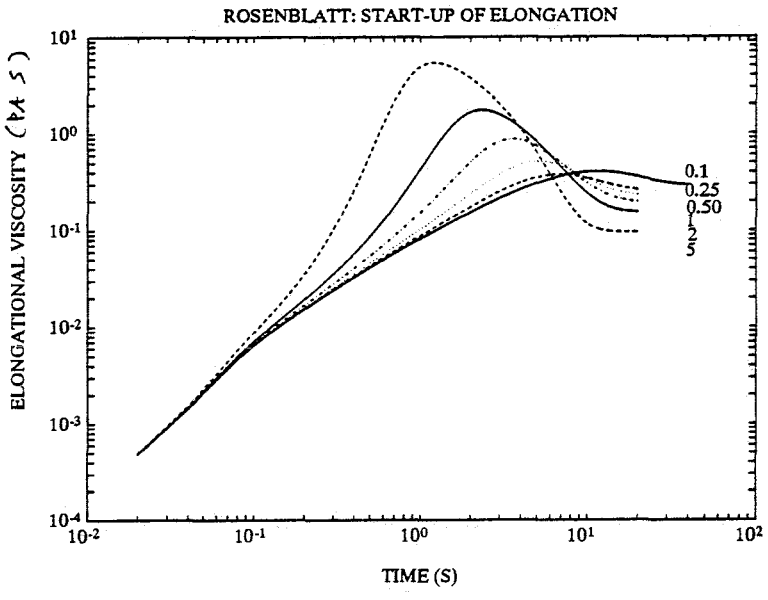

Figure 5.2 *Calculations with the Rosenblatt model in case of start-up of simple elongational flow. Six different elongational rate steps have been used (0.1, 0.25 , 0.50, 1, 2, 5 s^{-1}) with a ramp of 0.075 s.*

From Fig. 5.2 it appears that in start up of simple elongational flow the elongational viscosity has a maximum. This maximum is reached at a lower time when the elongation rate step increases at the same total elongation $\varepsilon=\dot{\varepsilon}t$. The curves with elongational rate steps 0.25, 0.50, 1, 2 and 5 s^{-1} show that the maximum increases when the elongational rate steps are increased. Only the case with a rate step to 0.1 s^{-1} has a larger value than the 0.25 and 0.50 s^{-1} cases. The influence of this maximum on 2D flow is not clear. Note that Fig. 5.1 follows from a vertical cut of Fig. 5.2 at large times.

5.4 Conclusions

Using the Rosenblatt model with α = 1.2 and k = 0.25 s^{-1} the Trouton ratio lies between 0.2 and 10 at deformation rates in the range 10^{-3} and 10^{3}.

In start up of simple elongation for rate steps from zero to elongation rates $\geq$ 1 s^{-1}

relatively high elongational viscosities are found.

To avoid singularities in the elongational viscosity the constraint $\alpha > 2/\sqrt{3}$ must be satisfied.

The parameter set $\alpha = 1.2$ and $k = 0.25\ s^{-1}$ for the single mode case satisfies the constraint $\alpha > 2/\sqrt{3}$.

Not all modes of the 5 mode fit in Chapt. 3 satisfy the constraint $\alpha > 2/\sqrt{3}$. As long as $\lambda_1 = 500$ s this constraint cannot be satisfied. However, with the small frequency interval of the measured complex viscosity of blood, $\lambda_1 = 500$ s gave the best fit of the complex viscosity (see Section 4.4). A smaller value of λ_1 ($O(10^1)$) is necessary to obtain a fit that satisfies the constraints for α_i.

6 Calculations in planar flow

6.1 Introduction

In Chapt. 4 and 5 we studied the behaviour of the Rosenblatt model in elementary one dimensional flow: simple shear and simple elongation flow. When possible, model predictions were compared with experimental data of human blood. All model parameters were determined from fits on shear stresses measured in simple shear flow. Good agreement was found between model predictions and experiments, which gives confidence in the model.

After that preparatory study this chapter continues with the calculation of two dimensional planar flow of blood. It is the first step towards the calculation of viscoelastic flow of blood in physiological situations.

The calculation of two dimensional flow using the Rosenblatt model to describe the time-dependent behaviour of the blood is a complex issue. In general, viscoelastic flow computations are far from standard and many different numerical approaches are currently experimented with.

In this chapter a mixed Finite Element Method (with operator splitting and a Time-discontinuous/ Galerkin-Least-Squares method) is used to solve the equation of motions combined with the Rosenblatt model as the constitutive equation. The basics of the method have been published by Baaijens [1992a] for Stokes flow with the Phan Thien Tanner and Giesekus models. Modifications for the Rosenblatt model and the addition of the convective term are subject of the study in this report.

The method described below is used for several reasons. First, it had proved to be succesful for the viscoelastic Phan Thien Tanner and Giesekus models (at a Weissenberg number of ≈ 1.6). Secondly, it can easily handle multi modes. And thirdly, it is an intrinsically unsteady technique. Hence, in principle, simulation of realistic pulsatile flow is possible.

First, the mathematical and numerical problem is defined in Section 6.2. Accordingly, in Section 6.3 the results are discussed for calculations of planar flow in an artery with a model stenosis with 25% area reduction. It will appear that the numerical method used can succesfully be applied for the problem considered. The program has a large potential for use in future studies. Finally some conclusions and recommendations are made in Section 6.4. It is emphasized, that the calculations presented here have a tentative character. More profound studies are necessary before strong conclusions can be made. In particular, extension should be made towards axisymmetric problems with pulsatile flow.

6.2 Problem definition

6.2.1 Strong form

The isothermal and incompressible flow of fluids is described by the conservation of momentum and conservation of mass, combined with a constitutive equation for the Cauchy stress tensor. Consider a domain of interest Ω in $\mathbb{R}^2$ with smooth boundary Γ, and the time interval $I =]0,T[$. To simplify the notation, we write $\underline{\tau}$ instead of $\underline{T}'_{st}$ for the structural dependent part of the extra stress tensor (cf. Chapt. 3).

The incompressible, unsteady planar flow of a Rosenblatt fluid is defined by the following problem (cf. Baaijens [1992a]):

Problem PRE *Given $\vec{u}^0$: $\Gamma_u \mapsto \mathbb{R}^2$, find the plane extra stress field $\underline{\tau}(\vec{x},t)$: $\Omega \times I \mapsto \mathbb{R}^{2\times2}$, velocity field $\vec{u}(\vec{x},t)$: $\Omega \times I \mapsto \mathbb{R}^2$, the pressure field $p(\vec{x},t)$: $\Omega \times I \mapsto \mathbb{R}$, for all $(\vec{x},t) \in \Omega \times I$, such that*

$$-\rho\left(\frac{\partial \vec{u}}{\partial t} + \vec{u}\cdot\vec{\nabla}\vec{u}\right) + \vec{\nabla}\cdot\left(-pI + 2\eta^{\infty}\underline{\mathcal{D}} + \sum_i \underline{\tau}_i\right) = \vec{0} \qquad i=1,N \qquad (6.1)$$

$$\vec{\nabla}\cdot\vec{v} = 0 \qquad (6.2)$$

with for the Rosenblatt model:

$$\frac{\partial \underline{\tau}_i}{\partial t} + \vec{u}\cdot\vec{\nabla}\underline{\tau}_i - \underline{L}\cdot\underline{\tau}_i - \underline{\tau}_i\cdot\underline{L}^T + \frac{1}{\lambda_i}\underline{\tau}_i = 2\frac{\eta_i}{\lambda_i}\underline{\mathcal{D}} \qquad i=1,N \qquad (6.3)$$

with

$$\lambda_i = P_i/k_i \qquad (6.4)$$

$$\eta_i = \eta^0 P_i \qquad (6.5)$$

$$\frac{\partial P_i}{\partial t} + \vec{u}\cdot\vec{\nabla}P = -k_i(1-P_i) + \alpha\dot{\gamma}P_i \qquad (6.6)$$

$$\dot{\gamma} = \sqrt{(2\underline{\mathcal{D}}:\underline{\mathcal{D}})} \qquad (6.7)$$

with $\underline{L} = (\vec{\nabla}\vec{v})^T$, while the following boundary conditions are specified on Γ ($= \Gamma_u \cup \Gamma_\tau$).

$$\vec{u}(\vec{x},t) = \vec{u}^0(\vec{x},t) \qquad \text{on } \Gamma_u \times I \qquad (6.8)$$

$$-pI + 2\eta^{\infty}\underline{\mathcal{D}} + \sum_i \underline{\tau}_i(\vec{x},t) = 0 \qquad \text{on } \Gamma_\tau \times I \qquad (6.9)$$

Operator splitting

An essential feature in the Finite Element Method used is the *operator splitting* technique. Define the material derivative operator $\mathcal{L}_t$:

$$\mathcal{L}_t = \frac{\partial}{\partial t} + \vec{u}\cdot\vec{\nabla} \qquad (6.10)$$

then the part of the constitutive equation that deals with the stresses (left hand side of Eq. (6.3)) can be splitted in two parts:

$$\mathcal{L} = \mathcal{L}_t + \mathcal{L}_R \qquad (6.11)$$

with

$$\mathcal{L}_R = -\boldsymbol{L}\cdot - \cdot\boldsymbol{L}^T + \frac{1}{\lambda_i} \qquad (6.12)$$

with $\frac{1}{\lambda_i} = \frac{k_i}{P_i}$ in case of the Rosenblatt model. Consider a quantity B (scalar, vector, tensor), than the operator $\mathcal{L}_t$ is defined formally as

$$\mathcal{L}_t B = \frac{\partial B}{\partial t} + \vec{u}\cdot\vec{\nabla}B = \frac{DB}{Dt} = \dot{B} = \lim_{\alpha\to 0}\frac{B(\vec{x},t+\alpha\Delta t)-B(\vec{p},t)}{\alpha} \qquad (6.13)$$

with $\vec{p}$ denoting the position at time t of the particle that is located at position $\vec{x}$ at time $t+\alpha\Delta t$. The equation

$$\frac{DB}{Dt} = 0 \qquad (6.14)$$

describes the convective transport of B only. It describes the transport of property B by flow, and is associated with material elements moving with the flow. During each time step, the material rates in the different model equations are dealt with separately from the remaining parts of the equations.

After splitting the time interval I into N_t time steps,

$$I = \bigcup_{n=1}^{N_t} I_n,\ I_n =]t_n^+, t_{n+1}^-[\qquad (6.15)$$

with

$$t_n^{\pm} = \lim_{\varepsilon \to 0^{\pm}} t_n \pm \varepsilon \qquad (6.16)$$

From Eq. (6.13) we approximate the material rate during I_n by

$$\mathcal{L}_t^n B = \frac{B(\vec{x}, t_{n+1}) - B(\vec{p}, t_n)}{\Delta t} \qquad (6.17)$$

6.2.2 Mixed weak form

If $\tau_i(\vec{p},t_n)$, $\vec{u}(\vec{p},t_n)$ and $P_i(\vec{p},t_n)$ are known, then for each time interval I_n the mixed weak formulation of problem PVE is given by

Problem MPRE *Given $\tau_i(\vec{p},t_n)$ $\vec{u}(\vec{p},t_n)$ and $P_i(\vec{p},t_n)$, find $(\tau_i,\vec{u},p) \in S \times U \times Q$ at $t=t_{n+1}$, such that for all $(s_i,\vec{v},q) \in S \times V \times Q$*

$$(s_i, \mathcal{L}_t^n \tau_i + \mathcal{L}_R \tau_i - 2(\frac{\eta_{0i}}{\lambda_i}) D_u) = 0 \qquad i=1,N \qquad (6.18)$$

$$-(\vec{v}, \rho \mathcal{L}_t^n \vec{u}) - (\mathcal{D}_v, 2\eta^{\infty}\mathcal{D} + \sum_i \tau_i) + (\vec{\nabla}\cdot\vec{v}, p) = 0 \qquad (6.19)$$

$$(q, \vec{\nabla}\cdot\vec{u}) = 0 \qquad (6.20)$$

$$\mathcal{L}_t^n P_i - (k_i + \alpha\dot{\gamma}) P_i + k_i = 0 \qquad \forall \text{ integration points} \qquad (6.21)$$

with the spaces U,V,Q,and S defined as follows: the velocity space U

$$U = \{ \vec{u} \mid \vec{u} \in [H^1(\Omega)]^2,\ \vec{u} = \vec{u}^0 \text{ on } \Gamma_u \} \qquad (6.22)$$

the velocity trial space V

$$V = \{ \vec{v} \mid \vec{v} \in [H^1(\Omega)]^2,\ \vec{v} = \vec{0} \text{ on } \Gamma_u \} \qquad (6.23)$$

the pressure (trial) space Q

$$Q = \{q |\ q \in L_2(\Omega)\} \tag{6.24}$$

the stress (trial) space

$$S = \{s |\ s \in [L_2(\Omega)]^{2\times 2}\} \tag{6.25}.$$

The initial condition for P_i is:

$$P_i = 1 \text{ on } t=0 \text{ on } \Omega \tag{6.26}$$

In Appendix A the different definitions for the inproduct (,) are given. The remaining problem is to determine $\vec{u}(\vec{p},t_n)$, and $\tau_i(\vec{p},t_n)$ and $P_i(\vec{p},t_n)$ for each mode.

6.2.3 Discretization of the transport problem with a Space-Time/Galerkin Least Squares Finite Element Method

In this section a Space-Time/Galerkin Least Squares Finite Element Method (cf. Baaijens [1992a]) is used in which not only space but also time is discretized in a finite element manner. For the time-discretization the space-time domain $\Omega \times I$ is divided into N_t space-time slabs:

$$\Omega \times I = \bigsqcup_{n=1}^{N_t} Q_n, \qquad Q_n = \Omega_n \times I_n, \qquad I_n =]t_n^+, t_{n+1}^-[\tag{6.27}$$

The time-discretization is chosen such that it is piecewise continuous but discontinuous across the space-time slabs, allowing each time slab to be analysed subsequently. The Space-Time/Galerkin Least Squares Finite Element Method with the time-discontinuous approximation applied to the transport problem (6.14) results in problem PTR (B: scalar, vector or tensor):

Problem PTR *Given $\vec{u}(\vec{x},t)$, $t \in I_n$, find $B_p \in D$ such that for all $\mathcal{B}_p \in D$ and $\beta > 0$*

$$[\mathcal{B} + \beta \mathcal{L}_t \mathcal{B},\ \mathcal{L}_t B] + (\mathcal{B}(t_n^+), (B_p(t_n^+) - B_n(t_n^-)) = 0 \tag{6.28}$$

The inproduct [,] is defined by (in case of a tensor field):

$$[B,B] = \int_{\Omega_n} B:B \, d\Omega \qquad (6.29).$$

An appropriate definition for the space D has to be made: in case of $B = \underline{\tau}$ the stress (tensor field):

$$D = \{\underline{\tau} \mid \underline{\tau} \in [\, H^1(\Omega)]^{2\times 2} \times I_n\} \qquad (6.30),$$

in case of $B = \vec{v}$ the velocity (vector field):

$$D = \{\, \vec{v} \mid \vec{v} \in [H^1(\Omega)]^2 \times I_n\} \qquad (6.31).$$

The mixed problem MPRE and the transport problem PTR are coupled. They are solved in a decoupled way with an iterative procedure. The nonlinear problem MPRE is solved with a Newton-Raphson iteration scheme (e.g., Baaijens [1992a]). At the beginning of each iteration first for $\underline{\tau}$, $\vec{v}$, and P the transport problem is solved, using the last previously computed approximation of the velocity field. This yields an estimate for $\underline{\tau}_p$, $\vec{v}_p$, and P_p that is required to solve problem MPRE.

It is important to note that the numerical technique described above is intrinsically unsteady. The solution procedure is started at t=0 s from rest, and the boundary conditions for the velocity are applied instantaneously at t=0 s. The steady solution is obtained from the limit solution at large times. Although this seems to be a cumbersome way for calculating steady flow, the calculation is more realistic in a physical sense. For in physical experiments steady flow is also obtained as the limit situation after the start up of flow. Likewise, when solving the steady Navier-Stokes equations, the non-linear problem has to be solved iteratively for a stepwise incremented Reynolds number.

6.2.4 Discretization

The domain Ω is divided in N_{el} elements:

$$\Omega = \bigcup_{e=1}^{N_{el}} \Omega^e \qquad (6.32).$$

The k-th order interpolation polynomial on a triangular, respectively quadrilateral element e is denoted with $P_k(\Omega^e)$ and $Q_k(\Omega^e)$ respectively. In this study the element $(s_i,\vec{u},p) \longrightarrow P_1^d Q_1 Q_0^d$ and $T \longrightarrow Q_1$ (the suffix d denotes a discontinuous interpolation) is used, which gives as finite element approximations of U,V,S,Q,S_{tr},V_{tr}:

$$U^h = \{ \vec{u}^h \mid \vec{u}^h \in [Q_1(\Omega)]^2, \vec{u}^h = \vec{u}^0 on\ \Gamma_u \} \qquad (6.33)$$

$$V^h = \{ \vec{v}^h \mid \vec{v}^h \in [Q_1(\Omega)]^2, \vec{v}^h = \vec{0}\ on\ \Gamma_u \} \qquad (6.34)$$

$$S^h = \{ s^h \mid s^h \in [P_1^d(\Omega)]^{2\times 2} \} \qquad (6.35)$$

$$Q^h = \{ q^h \mid q^h \in [Q_0^d(\Omega)] \} \qquad (6.36)$$

$$S_{tr}^h = \{ T_{tr}^h \mid T_{tr}^h \in [Q_1(\Omega)]^{2\times 2} \times P_0 \} \qquad (6.37)$$

$$U_{tr}^h = \{ \vec{v}_{tr}^h \mid \vec{v}_{tr}^h \in [Q_1(\Omega)]^2 \times P_0 \} \qquad (6.38)$$

Thus a piece-wise linear interpolation is used to approximate the extra stress tensor, that is discontinuous across element boundaries. In the transport problem a continuous bi-linear interpolation is used. In case of the stress field τ_p this approximation is first projected on a discontinuous P_1^d field on each element by a least squares projection. This field is used in problem MPRE.

6.3 Calculation of planar flow through a stenosed artery

Using the numerical method described above the planar flow of blood through an artery with a stenosis in case of the Rosenblatt model was calculated with the single mode veersion with $\alpha = 1.2$ and $k = 0.25\ s^{-1}$. Although axisymmetry would be more realistic, planar flow was considered because the computer program was only suited for that.

Fig. 6.1 shows the geometry with the finite element mesh. The stenosis has a cosine shape. This type of model stenosis has been subject of many experimental and numerical Newtonian studies, e.g., Ahmed and Giddens [1983a],[1983b], Nakamura et al [1988]. Hence it provides a comparison for our results. However, here it is strongly emphasized that reservations must be made because these studies mentioned are axisymmetric instead of planar.

Furthermore, "sharp edged" or "contour edged" (cosine) stenoses produce different flow

phenomena, as was experimentally found by for example Cassanova and Giddens [1978] in a Newtonian study. Moreover, experience with viscoelastic flow computations has learned that,

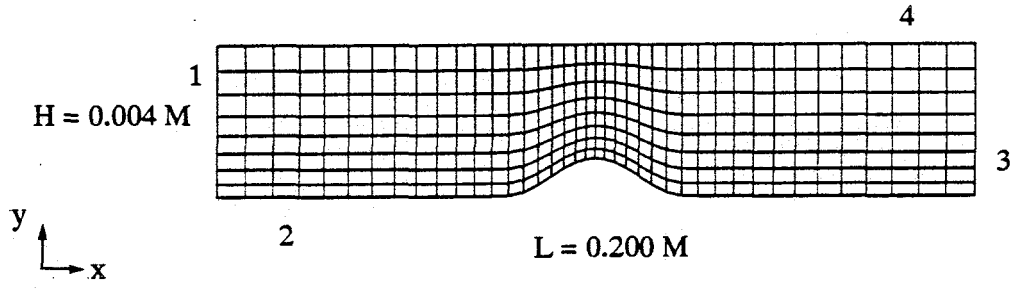

Figure 6.1 *Lower half of the geometry of a two dimensional artery with a cosine shaped stenosis with height D/8 and length 12D. Finite element distribution: 8 by 40 elements, 329 mesh points, 2632 degrees of freedom. The y-axis is multiplied with a scale factor 10. Numbers indicate boundary numbers. Boundary conditions are (with velocity $\vec{u}$ = (u,v)): along entrance boundary Γ_1: $u = 6\bar{u}(y-D)y$, $v = 0$ with D: diameter of the artery and $\bar{u}$ = average velocity, wall Γ_2: $\vec{u} = \vec{0}$, exit boundary Γ_3: $v = 0$, and symmetry axis Γ_4: $u = 0$.*

as expected, sharp edges can produce numerical problems that are avoided by using a cosine shaped stenosis. Note that the stenosis has a relative large length. Other studies, e.g., Ahmed and Giddens [1983a], used a stenosis with length 2D. A stretched cosine with length 12D was chosen as a starting point for viscoelastic calculations.

The calculations have two major goals. The first aim is to investigate whether a solution could be obtained anyway for the flow problem considered using the described numerical method combined with the Rosenblatt model. The second reason was to analyse the influence of the constitutive model (Rosenblatt vs. Newtonian) in steady flow. Unfortunately, at the time this report had to be finished, no results of a Newtonian calculation were yet available. Detailed comparisons will be made in the near future. Some comparisons are made in this report with results from literature.

Boundary conditions were (with velocity $\vec{u}$ = (u,v)): along entrance boundary Γ_1: $u = 6\bar{u}(y-D)y$, $v = 0$, with D: heigth of the channel (artery) and $\bar{u}$ = average velocity (fully

developed Newtonian flow), wall Γ_2: $\vec{u} = \vec{0}$ (no slip), exit boundary Γ_3: v = 0, and symmetry axis Γ_4: u = 0. After some experimenting, entrance and exit sections were chosen sufficiently large such that fully developed flow conditions were reached (as is proved a posteriori by the solution). The Reynolds number was calculated from (Liepsch and Moravec [1983]):

$$Re = \frac{\bar{u}D\rho}{\bar{\eta}} \tag{6.39}$$

with $\bar{u}$ the mean fluid velocity and $\bar{\eta}$ a characteristic viscosity. This viscosity $\bar{\eta}$ is calculated from $\bar{\eta} = \tau(\bar{\dot{\gamma}})/\bar{\dot{\gamma}}$ with $\bar{\dot{\gamma}}$ a characteristic shear rate: $\bar{\dot{\gamma}} = \frac{2\pi\bar{u}}{D}$. According to Rindt [1989], during pulsatile physiological flow in the human carotid artery bifurcation the mean value of the Reynolds number in case of Newtonian flow equals 300 (see Section 2.4).

In viscoelastic flow, a second dimensionless number is of importance: the Weissenberg number that represents the ratio of elastic and viscous forces. It is defined by:

$$We = \frac{\lambda_f \bar{u}}{D} \tag{6.40}$$

with λ_f a characteristic fluid time. In case of the Rosenblatt model, a characteristic fluid time λ_f can be defined by

$$\lambda_f = \dot{P}/k = 1/(k+\alpha\frac{\bar{u}}{D}) \tag{6.41}.$$

Hence:

$$We = \frac{\bar{u}}{D}/(k+\alpha\frac{\bar{u}}{D}) \tag{6.42}$$

(in the limit $\bar{u} \to \infty$, $We \to 1/\alpha$). Note that Re and We cannot be chosen independently. Many authors report that above a certain critical Weissenberg number the numerical solutions do not converge. With the method used here, it is not yet known if such a limit exists.

With Re = 100 a solution was obtained without any problem. From the above formulas for Re and We with D = 0.008 m, ρ = 1050 kg/ms^2, it follows that $\bar{u}$ = 0.051 (m/s), and thus We = 0.80 (λ_f = 0.13). This agrees with the estimation λ = 0.1, We = 1 in Section 2.4.

The element distribution is plotted in Fig. 6.1 (with vertical axis multiplied with a scale factor 10). The mesh is chosen such that the element size in the transverse direction was minimal along the wall, and also minimal in longitudinal direction near the stenosis, where velocity gradients are expected to be maximal.

Computations were performed on a Silicon Graphics Personal Iris Workstation. Time discretisation was chosen with the following time steps: 4 steps of 0.001 s, 3 of 0.002 s, 4 of 0.01 s, 3 of 0.02 s, 4 of 0.1 s, 3 of 0.2 s, 12 of 0.25 s, and 8 steps of 1 s. In total 41 time points were used, with t_{end} = 12 s. The total number of iterations used was 140. The choice for t_{end} was made such that the solution was stationairy in time. This was verified by comparing the stresses at t=11 s and t=12 s, which differed less than 1 %.

One complete calculation took about 14 hours. This large computation time is mainly caused by the fact that the program is written in terms of MATLAB routines (MATLAB [1990]). Experience has shown that the speed of this kind of programs can be improved with a factor 20 when routines are written in, for example, the language C. We did not calculate the problem for a refined mesh because this would increase computing time enormously.

6.3.1 Steady flow

First, we discuss the results in steady flow. The fully developed velocity profile for the Rosenblatt constitutive model is compared with the result for the Newtonian model.

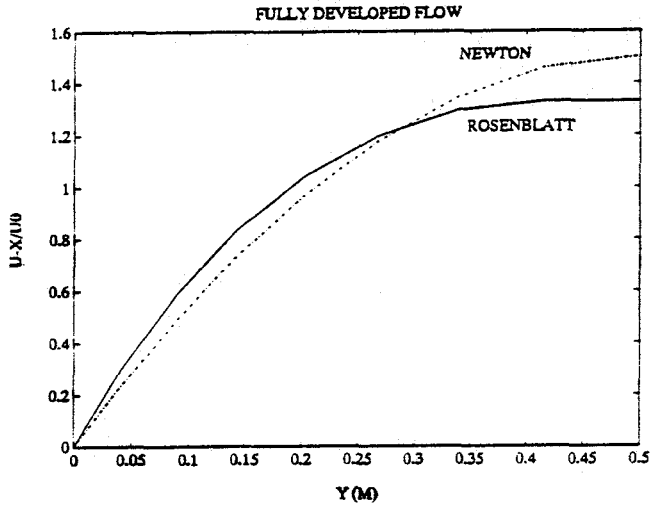

Figure 6.2 *Velocity profiles for fully developed flow of a Newtonian fluid (– ·), and of a Rosenblatt fluid (—).*

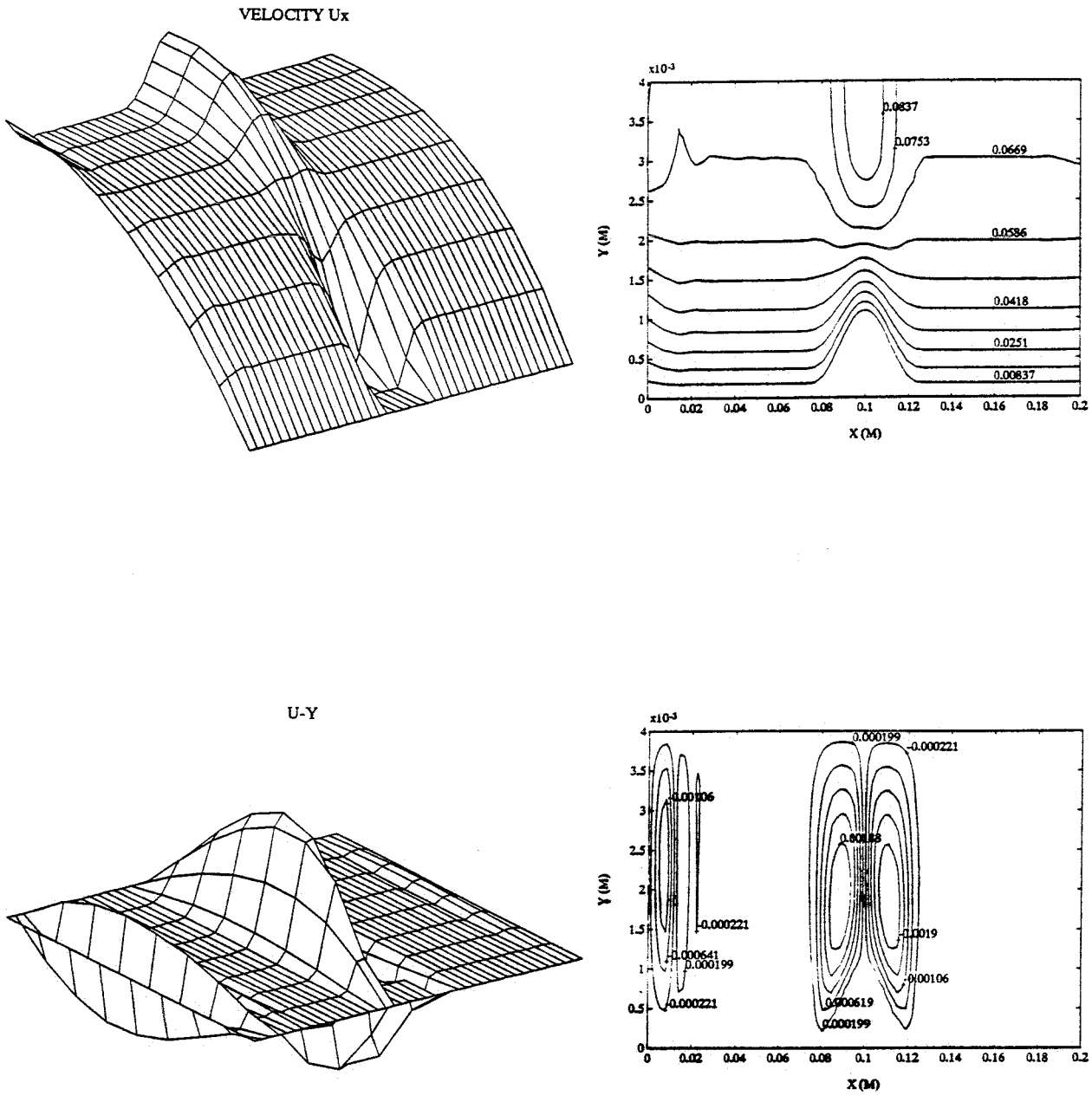

Figure 6.3 *Velocities in planar flow through an artery with a mild stenosis with 25 % area reduction calculated with the Rosenblatt model (all velocities in contour plots in units m/s).*

Results are shown in Fig. 6.2, with the Rosenblatt profile obtained from results of the numerical calculation in the exit section (no analytical solution can be found for a fully developed velocity profile in case of the Rosenblatt model). The influence of the shear thinning behaviour of the Rosenblatt model is clear: a flatter velocity profile with a lower maximum value at the symmetry axis.

Fig. 6.3 shows the results for the velocities u and v. All mesh plots in this section were made using an equally spaced interpolation mesh that had the same number of elements in x and y direction as the original mesh. Notice that the ratio of the lenght of the plots in x and y direction are not the same as the real case (where L/H = 50 (see Fig. 6.1)). All units in the contour plots are SI units, thus Pa for stresses and m/s for velocities.

As expected, due to the inflow boundary condition and geometry variation (stenosis), all plots in Fig. 6.3 have two areas that show strong local changes in velocities.

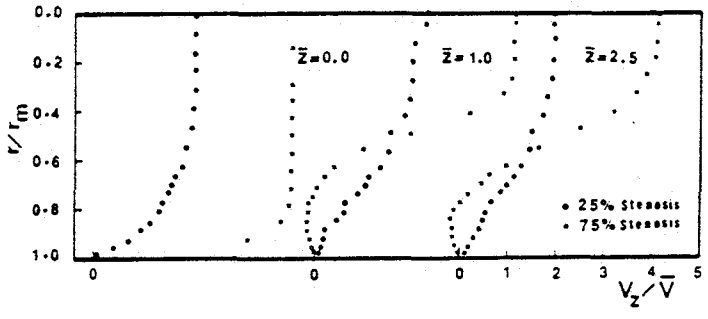

Figure 6.4 *Axial velocities at several positions after an axial symmetric stenosis with 25 % and 75 % area reduction in steady Newtonian flow at Re = 500 ($\bar{Z}$ = Z/D, Z = distance from center of stenosis, D = diameter unstenosed artery) (from Ahmed and Giddens [1983a]).*

First, in the entrance section development of the Newtonian profile to the fully developed velocity profile of the Rosenblatt model results in a decreasing maximum value of u on the symmetry axis, an oscillation (from zero to negative, then to positive and back to zero) in the velocity v. After this entrance effect all velocities attain a steady value.

Secondly, at the symmetry axis near the stenosis the velocities have elevated values. The velocity u is increased by the narrowing of the artery with 25%. The velocity v is zero in

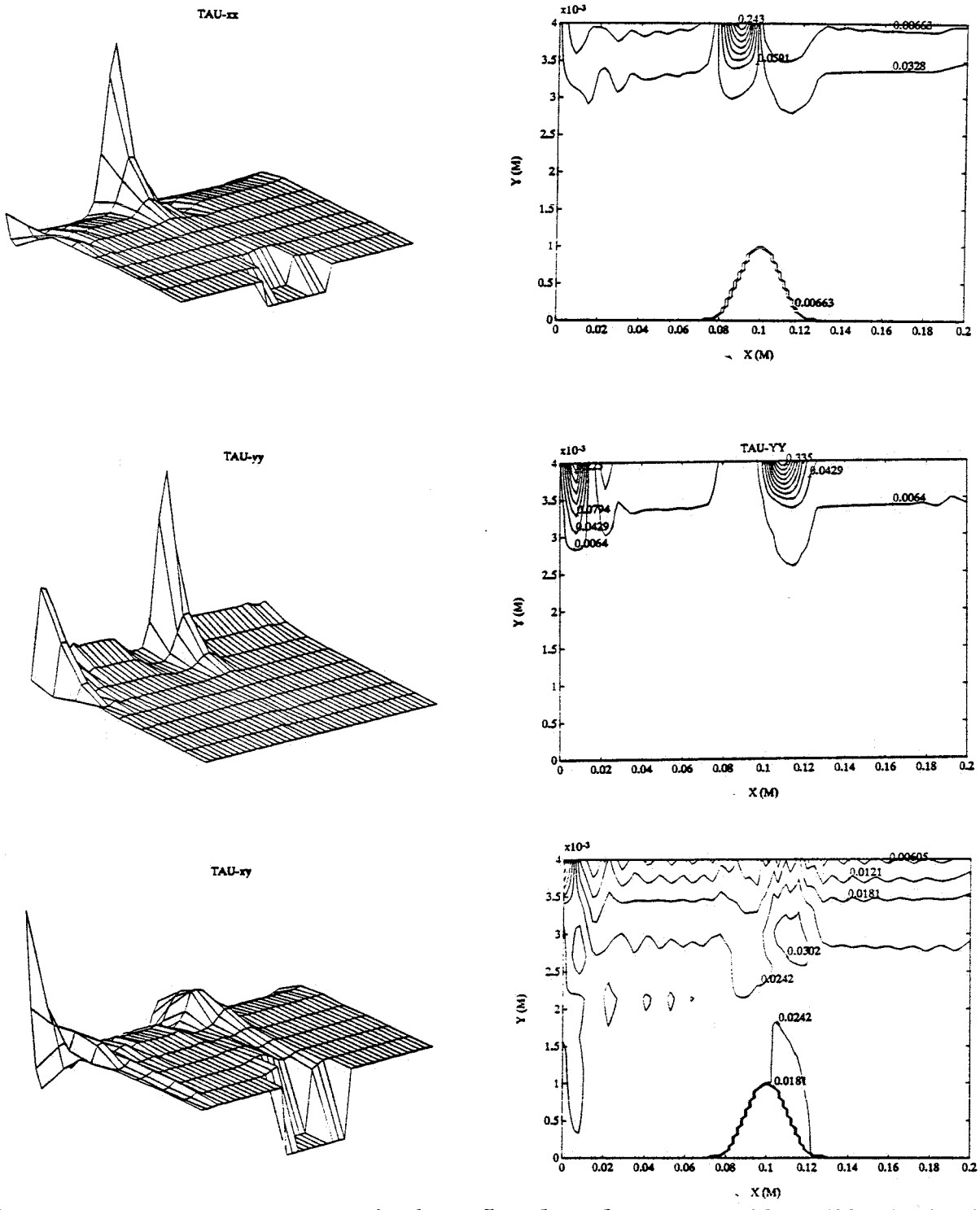

Figure 6.6 *Extra stresses in planar flow through an artery with a mild stenosis with 25 % area reduction calculated with the Rosenblatt model (all stresses in contour plots in units Pa).*

the area with fully developed flow before and after the stenosis. A positive velocity v is found at the rising part of the stenosis, and negative at the back of the stenosis.

From the fact that the velocity u is always positive, no flow recirculation area is present after the stenosis. Emphasizing that reservations must be made when comparing results in planar flow with those in axisymmetry, this is a similar result as the experimental results of Ahmed and Giddens [1983a] who found no flow recirculation and a laminar, stable flow field behind the stenosis for a Reynolds number below 1000 in case of the Newtonian flow through an artery with an axisymmetric cosine stenosis with 25 % area reduction. On the contrary, in case of a model stenosis with 75 % area reduction a flow recirculation was found indeed already at Re=500 (Fig. 6.4). This can be an interesting problem for future study.

The calculated extra stresses τ_{xx}, τ_{yy}, and τ_{xy} are plotted in Fig. 6.6. As with the velocities, strongest effects are found near the entrance boundary (that are trivial) and near the stenosis. It is important to realise that in case of the Rosenblatt model the stress τ_{xy} is no longer a simple function of $\frac{\partial u}{\partial y}$ solely, as it is in case of the Newtonian model. This can be seen in steady flow where the Rosenblatt model gives as equations for τ_{xx}, τ_{yy}, and τ_{xy} respectively:

$$(1-2\lambda(\frac{\partial u}{\partial x}))\tau_{xx} = 2\lambda(\frac{\partial u}{\partial y})\tau_{xy} + 2\eta(\frac{\partial u}{\partial x}) \tag{6.43}$$

$$(1-2\lambda(\frac{\partial v}{\partial y}))\tau_{yy} = 2\eta(\frac{\partial v}{\partial y}) + 2\lambda(\frac{\partial v}{\partial x})\tau_{xy} \tag{6.44}$$

$$(1-\lambda(\frac{\partial v}{\partial y})+(\frac{\partial u}{\partial x}))\tau_{xy} = \lambda(\frac{\partial u}{\partial y})\tau_{xx} + \lambda(\frac{\partial u}{\partial y})\tau_{yy} + \eta((\frac{\partial u}{\partial y})+(\frac{\partial v}{\partial x})) \tag{6.45}$$

with $\eta = \eta_0 k^2/(k+\alpha\dot{\gamma})$, $\lambda = \eta_0/(k+\alpha\dot{\gamma})$, and $\dot{\gamma} = ((\frac{\partial u}{\partial x})^2 + \frac{1}{2}((\frac{\partial u}{\partial y})+(\frac{\partial v}{\partial x}))^2+(\frac{\partial v}{\partial y})^2)^{\frac{1}{2}}$.

6.3.2 Start up of steady flow

The steady solution as dicussed in the previous section was the final result of the numerical solution procedure at t=12 s. In this section the transient behaviour of blood during start up of flow between t=0 s and t=12 s is analysed. Results were saved at t= 0.001, 0.004, 0.01, 0.04, 0.1, 0.4, 1, 2, 3, 4, 6, 8 and 12 s. In all mesh plots presented in this section, the time axis has no real scale, but simply indicates the subsequent results that have been saved. The lack of desired plot routines is due to the experimental stage of the computer program used. The time scale used here is almost logarithmic, in particular for t< 1s.

In the following the results for u, τ_{xx}, τ_{yy}, and τ_{xy} will be discussed successively. Figure

6.7 shows the velocity profiles of u along a vertical line through the top of the stenosis. As in all plots presented below, the dot indicates the position of the wall and the arrow the positive direction of the time axis.

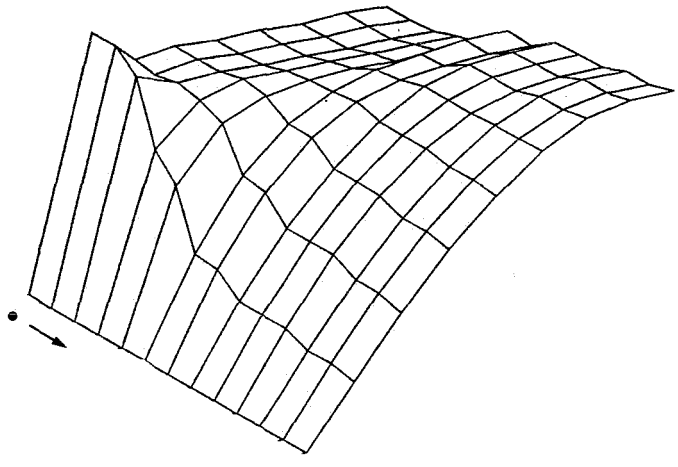

Figure 6.7 *Velocity u in x direction along vertical line through flow at the top of the stenosis, as function of time. The dot indicates the location of the wall, and the arrow the direction of the positive time axis.*

Fig. 6.8 shows the development in time of the velocity u along a vertical line through the flow on top of the stenosis. Note that here at t=2 s the steady solution for u is reached. Maximum value is 0.092 m/s.

The development of extra stresses in time are presented along the symmetry axis, along the wall. Fig. 6.8a shows the stresses τ_{xx} along the wall. Clearly, after t=6 s, the steady solution is reached. Note the similarity with stress growth after a shear rate step in simple shear flow (Chapt. 4): a stress overshoot immediately after start up of flow. Maximum value is 0.6370 Pa.

The growth in time of stresses τ_{xx} along the center axis are plotted in Fig. 6.8b. Along this line the stresses start to grow at t = 0.4 s, instead at t=0.001 s as it is the case along the wall. Maximal value is 0.2705 Pa.

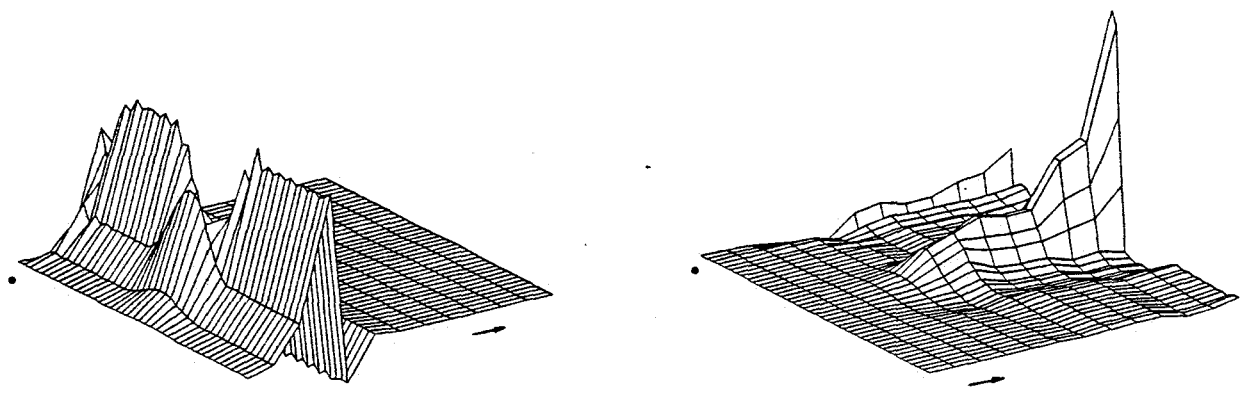

a) b)

Figure 6.8 *Growth in time of stresses τ_{xx} along a) the wall, b) the symmetry axis.*

In a similar way, the growth of stresses τ_{yy} is plotted in Fig. 6.9 a) and b). In a) the maximal value is 0.012 Pa, and in b) 0.55 Pa. Clearly, along the wall immediately the stresses τ_{yy} grow, and have an overshoot at the position of the stenosis. As with τ_{xx} in Fig. 8, the

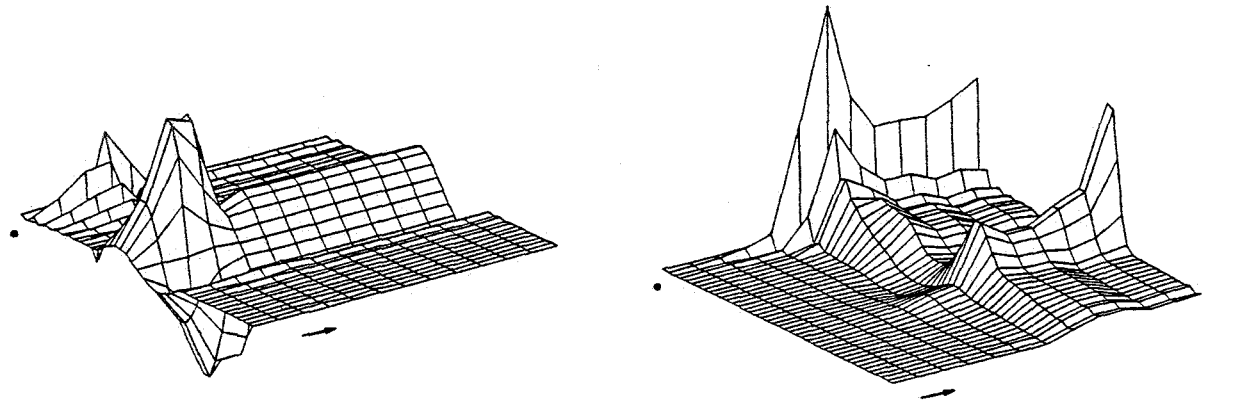

a) b)

Figure 6.9 *Growth in time of stresses τ_{yy} along a) the wall, b) the symmetry axis.*

development of stresses τ_{yy} is slower along the symmetry axis (it starts at t=0.4 s) than along the wall (at t=0.001 s). Also, along the wall a stress overshoot is found at $t < 0.1$ s, while this is not the case along the symmetry axis. At the wall, the stresses τ_{yy} reach a steady value already at t=0.4 s.

Stresses τ_{xy} are plotted along the wall in Fig. 6.10. Here τ_{xy} shows an overshoot between t=0 and t=0.4 s; at larger times the solution attains a steady value. The maximum value is 0.19 Pa. At the symmetry axis the stresses τ_{xy} are zero.

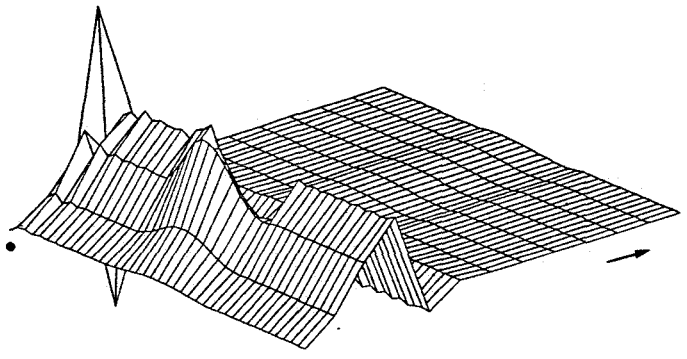

Figure 6.10 *Growth in time of stresses τ_{xy} along the wall.*

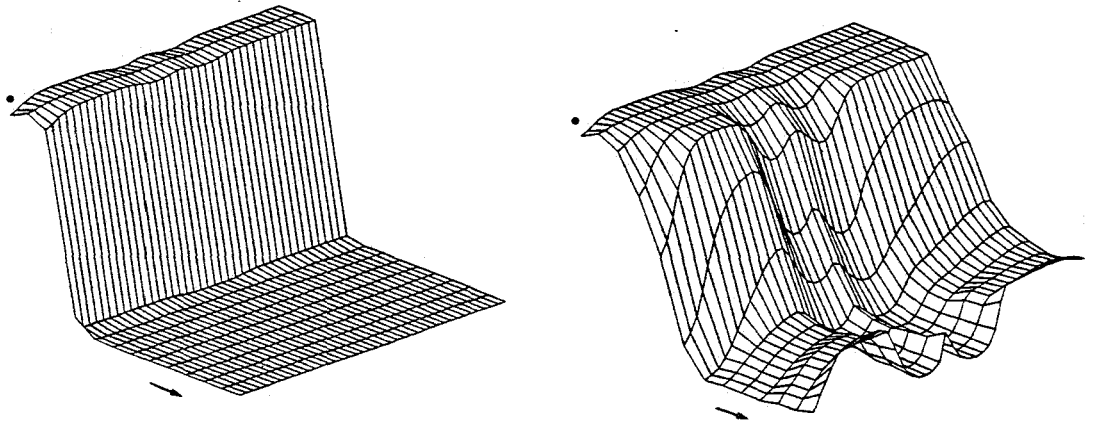

a b

Figure 6.11 *Change in time of the structure parameter P in the Rosenblatt model a) at the wall, and b) at the symmetry axis.*

In Fig. 6.11 the change in time during start up of flow of the structure parameter P in the Rosenblatt model has been plotted, both along the wall and at the symmetry axis. Clearly, as with the stress components discussed above, at the wall the steady solution is reached much faster than at the symmetry axis. Here, at the wall it is reached already at t=0.04 s, while at the symmetry axis the steady value is reached at t=3 s. This can be explained by the fact that the structure parameter P decreases with increasing shear rate, that is maximal at the wall.

6.4 Conclusions

The fully developed velocity profile of the Rosenblatt model differs from the Newtonian profile as the shear thinning generalized Newtonian models do: a flatter velocity profile with a lower maximum velocity.

The numerical method described in this chapter has been succesfully applied for the solution of steady planar flow through a stenosed artery.

From the results during start up of flow, it is concluded that the Rosenblatt model predicts a much faster response of the extra stresses τ_{xy}, τ_{yy}, τ_{xx} and the structure parameter P parameter is found along the wall (steady situation within 0.4 s) than at the symmetry axis (within 3 s). This can be explained by the shear rate dependence of the stresses and the parameter P. At the wall, the velocity gradients (and thus shear rates) are much larger than at the symmetry axis.

The first steps in future studies with these type of calculations that should be made are: - comparison of the results of the Rosenblatt model in start up of flow with Newtonian calculations; -influence of Reynolds number: a higher Reynolds number (300) is more representative as a mean value for physiological flow; - influence of stenosis geometry: height, length and/or shape of stenosis can be varied;- extension to axisymmetry and pulsatile flow: this gives a more realistic modeling of physiological artery flow, and also, in pulsatile flow the time-dependent character of the Rosenblatt model is expected to be of more influence. In particular, the influence of the Rosenblatt model on the existence and size of the flow recirculation area is of interest, because in that flow situation the viscoelastic character of the model is expected to be relevant.

To obtain a more detailed knowledge of the flow field, the pressure and the wall shear stress distribution should be investigated too.

For a better founded analysis of the problem considered, a calculation with a refined mesh is necessary. However, the software written in MATLAB gives rise to very long computation times. Also, in case of pulsatile flow with time-dependent boundary conditions,

computation times are expected to increase tremendously. Therefore, it is recommended to rewrite the program in a language like Fortran or C.

It is recommended for future use of this program to adjust it to the SEPRAN package. This has several advantages: it is faster (Fortran), accessible for a larger group of users, and has more plot routines available.

7 Conclusions and recommendations

Calculated shear stresses in simple shear flow, during a loading program that consists of two constant shearing time zones each followed by a non-shearing time zone, agree well with experimental data in case of shear rates of 8, 23 and 30 s^{-1}.

In steady shear flow the model gives a first normal stress difference that is smaller than the measurement accuracy of Copley and King [1975] and a second normal stress difference that is zero. This at least does not contradict experimental data.

A five mode version of the model improved the fit of the steady viscosity curve significantly. It also fitted the measured complex viscosity of human blood well (in the limit of linear viscoelastic behaviour the model changes into a linear Maxwell model). However the five mode version has two modes with singularities in the elongational viscosity. This might cause unrealistic, infinite high stresses in flows with recirculation areas.

More measured data of blood are necessary to verify model calculations, especially in flows other than simple shear. To improve the multi mode fit, the complex viscosity of blood should be measured over a broader frequency range. Also experimental data in elongational flow is needed to find a fit of the model parameters that is reliable in a broad range of flow types. However, measurements in simple elongation are extremely difficult to perform. Therefore flows with mixed shear and elongational deformation should be used.

In two respects the Rosenblatt model violates simple fluid theory. First, the retardation term $2\eta^{\infty}\mathbf{D}$ causes that strain steps cannot be described with the Rosenblatt model, because it would lead to infinite stresses. Secondly, the transition between linear and non-linear response of the model in an oscillating simple shear flow depends on the shear rate instead of on shear strain only. This disagrees with simple fluid theory too.

The calculations of the flow of blood in a planar model of a stenosed artery using the Rosenblatt model show that the numerical method used (a Finite Element Method with operator splitting and a Time-discontinuous/Galerkin Least Squares method) can succesfully be applied for this problem.

The numerical method is intrinsically unsteady. The program should be extended to axisymmetric problems. In particular, the behaviour of the Rosenblatt model in flow situations with flow recirculation areas should be investigated. In axisymmetric flows with flow recirculation, comparisons with Newtonian results are of high importance. Extension to pulsatile and three dimensional problems will complete the picture.

To reduce computation time substantially, it is necessary to rewrite the computer program now available in Fortran or some other language instead of MATLAB [1984].

More detailed comparative studies, both numerically and experimentally, are necessary to reveal the relevance of the non-Newtonian behaviour of blood on the three dimensional time-dependent flow phenomena in the human carotid artery bifurcation. In particular, research must first be focused at the experimental validation of numerical simulations, which needs for practical reasons a good rheological analog fluid for human blood. The Separan mixture with DMSO particles mentioned by Liepsch [1991b] and transparant slurries described by Mannheimer et al [1989] appear to be the best candidates for future studies.

References

Ahmed, S.A., Giddens, D.P, Velocity measurements in steady flow through axisymmetric stenoses at moderate Reynolds numbers, J. Biomechanics, Vol. 16, 7: 505-516, 1983a.

Ahmed, S.A., Giddens, D.P, Flow disturbance measurements through a constricted tube at moderate Reynolds numbers, J. Biomechanics, Vol. 16, 12: 955-963, 1983b.

Baaijens, J.P.W., A literature research into the rheology of human blood WFW-Report no. WFW-90.065, Eindhoven University of Technology, Eindhoven, The Netherlands, 1991.

Baaijens, F.P.T., Applied Computational Mechanics 2, Eindhoven University of Technology, The Netherlands, 1992a.

Baaijens, F.P.T., Application of Galerkin-Least-Squares related methods to the mixed formulation of viscoelastic flow, Part 3: unsteady flow with discontinuous interpolation, Submitted for publication in Journal of non-Newtonian Fluid Mechanics, 1992b.

Baaijens, J.P.W., v. Steenhoven, A.A., Janssen, J.D., Numerical analysis of steady generalized Newtonian blood flow in a 2D model of the carotid artery bifurcation, Submitted for publication in Biorheology, 1992c.

Bharadvaj, B.K., Mabon, R.F. and Giddens, D.P., Steady flow in a model of the human carotid bifurcation, Part 1-Flow visualization, Part 2-Laser-Doppler anemometer measurements, J. Biomechanics 15, 349-378, 1982.

Bernadin, D., Guillaume, S., Lucius, M., Fluides viscoélastique. Intégration du modèle de Carreau. Application à la rhéologie du sang, (Utilization of the Carreau model-B to describe periodic shear flow. Application to blood rheology), Journal de Mécanique théorique et appliquée, vol. 4, No. 4; 505-536, 1985.

Bernadin, D., PhD thesis, Institut National Polytechnique de Lorraine, Nancy, 1986.

Bernadin, D., Guillaume, S., Lucius, M., Un modèle rhéologique pour le sang comme mélange d'un fluide viscoélastique et d'un fluide visqueux (A rheological model for blood as a mixture of a viscoelastic fluid and a viscous fluid), Journal de Mécanique théorique et appliquée, vol. 6, No. 5; 647-662, 1987.

Caro, C.G., Pedley, T.J., Schroter, R.C., Seed, W.A., The mechanics of the circulation, Oxford, Oxford University Press, New York, Toronto, 1978.

Charara, J., Aurengo, A., Lelievre, J.C., Lacombe, C., Quantitative characterization of blood rheological behavior in transient flow with a model including a structure parameter, Biorheology, 22, 6; 509-519, 1985.

Chien, S., Blood rheology, in: Quantitative cardiovascular studies, eds. N.H.C. Hwang, D.R.

Gross and D,J. Patel, 241-287, Baltimore, University Park Press, 1979.

Cho, Y.I., and Kensey, K.R., Effects of the non-Newtonian viscosity of blood on flows in a diseased arterial vessel, Part1: steady flows, Biorheology, 28:241-262,1991.

Copley, A.L., King, R.G., On the viscoelasticity of anticoagulated whole human blood in steady shear as tested by rheogoniometric measurements of normal forces, Biorheology 15, 5-10, 1975.

Fukada, E., Seaman, G.V.F., Liepsch, D., Lee, M., Friis-Baastad L., Blood modeling using polystyrene microspheres, Biorheology, 26; 401-413, 1989.

Hoitinga, O., De numerieke simulatie van de stroming van visco-elastische materialen waarbij het materiaal beschreven wordt door een integraalmodel (in Dutch), master thesis, report number MEAH-88, Delft University of Technology, The Netherlands, 1990.

Hulsen, M.A.,Analysis and numerical simulation of the flow of viscoelastic fluids, PhD thesis, Delft University of Technology, Delft University Press, The Netherlands, 1988.

Hulsen, M.A., A numerical method for solving steady 2D and axisymmetrical viscoelastic flow problems with an application to inertia effects in contraction flows, report MEMT 11 of Delft University of Technology, The Netherlands, 1990.

Ku, D.N., Giddens, D.P., Laser Doppler Anemometer measurements of pulsatile flow in a model carotid bifurcation, J. Biomechanics, vol. 20, 407-421, 1987.

Ku, D.N., Liepsch, D., The effects of non-Newtonian viscoelasticity and wall elasticity on flow at a 90° bifurcation, Biorheology, 23; 359-370, 1986.

Larson, R.G., Constitutive equations for polymer melts and solutions, Butterworths, Boston 1988.

Lawson, C.L., Hanson, R.J., Solving Least Squares Problems, Prentice-Hall, Chapt.23, p161, 1974.

Liepsch, D., Fortschritt-berichte VDI, Strömungsuntersuchungen an modellen menschlicher blutgefäss-systeme; Reihe 7: strömungstechnik nr. 113, 1987.

Liepsch, D., Flow studies in a rigid T-junction model with a non-Newtonian fluid using a 3-D Laser-Doppler Anemometer, Proceedings 2nd International Conference on Biofluids and Biomechanics, Munich, june 1989.

Liepsch, D., Thurston, G., Lee, M., Studies of fluids simulating blood-like rheological properties and applications in models of arterial branches, Biorheology, 28; 39-52, 1991a.

Liepsch, D., Flow visualisation and 3D LDA measurements in models of arterial bifurcations, on: "Three dimensional blood flow in bifurcations, compuational and experimental analyses and clinical applications", Euromech Colloquium 286,Kerkrade, The Netherlands, october 20-23, 1991b.

Mann, D.E., Tarbell, J.M., Flow of non-Newtonian blood analog fluids in rigid curved and

straight artery models, Biorheology, 27; 711-733, 1990.

Mannheimer, R.J., Park, J.T., Grimley, T.A.,Morrow, T.B., Development and characterization of transparant slurries for basic and applied research in solids transport, Proceedings of fluids engineering seminar, Korea-U.S. Progress (held at Taelon, Korea, September, 3-8, 1989), pp. 483-506, 1989.

MATLAB, PC MATLAB manual, The MathWorks Inc.,South Natick, MA 01760, USA, 1989.

McMillan, D.E., Strigberger, J., Utterback, N.G., Rapidly recovered transient flow resistance: a newly discovered property of blood, Am.J. Physiology, 253, H919-H926, 1987.

Müller, I, On the frame dependence of electric current and heat flux in a metal, Acta Mechanica, 24:117-128,1976.

Nakamura, M., Sawada, T., Numerical study on the flow of a non-Newtonian fluid though an axisymmetric stenosis, Journal of Biomechanical Engineering, Transactions of the ASME, vol. 110; 137-143, 1988.

Press, W.H., Flannery, B.P., Teukolsky, S.A., Vetterling, W.T., Numerical Recipes, The art of scientific computing, Cambridge University press, Cambridge, 1987.

Rindt, C.C.M., Analysis of the three dimensional flow field in the carotid artery bifurcation, PhD thesis Eindhoven University of Technology, The Netherlands, 1989.

Rindt, C.C.M., van Steenhoven, A.A., Reneman, S., An experimental analysis of the flow field in a three-dimensional model of the carotid artery bifurcation, J. Biomechanics, 21:985-991, 1988.

Rosenblatt, J.S., Soong, D., Williams, M.C., A statistical mechanics theory for blood rheology: the rouleaux contribution, American Institute of Chemical Engineers, National Meeting 1986, Publ. by AIChE, New York, NY, USA Pap 90a, 29p, 1986.

Rosenblatt, J.S., The rheology of human blood: a structured fluid approach based on rouleau behaviour, PhD Thesis University of California, Berkeley USA, 1988.

Schmitz, E., Merzkirch, W., A test fluid for simulating blood flows, Experiments in fluids 2; 103-104, 1984.

Segal, G., Sepran User Manual, ingenieursburo SEPRA, Leidschendam, The Netherlands, 1984.

Steenhoven, van A.A., Reologie en microcirculatie (in Dutch), Eindhoven University of Technology, The Netherlands, 1984.

Tanner, R.I., Engineering rheology, Clarendon Press, Oxford, 1985.

Thurston, G.B., Frequency and shear rate dependence of viscoelasticity of human blood, Biorheology, 10; 375-381, 1973.

Thurston, G.B., Rheological parameters for the viscosity viscoelasticity and thixotropy of blood, Biorheology, 16; 149-162, 1979.

Thurston, G.B., Rheological analogs for human blood in large vessels, 2nd International Symposium on Biofluid Mechanics and Biorheology in Large Blood Vessels, Munich, june 25-28, 1989.

Vosse, v.d. F.N., Steenhoven, v. A.A., Janssen, J.D., Reneman, R.S., A two dimensional numerical analysis of unsteady flow in the carotid artery bifurcation (A comparison with three dimensional in-vitro measurements and the influence of minor stenoses), Biorheology, 27, 163-189, 1990.

Appendix A Definition of inproducts

Inproducts are defined by:

$$(a,b) = \int_{\Omega} ab \, d\Omega$$

if a,b are scalars,

$$(\vec{a},\vec{b}) = \int_{\Omega} \vec{a}\cdot\vec{b} \, d\Omega$$

if $\vec{a},\vec{b}$ are vectors, and:

$$(\boldsymbol{A},\boldsymbol{B}) = \int_{\Omega} \boldsymbol{A} : \boldsymbol{B} \, d\Omega$$

if $\boldsymbol{A},\boldsymbol{B}$ are tensors.